

UC Riverside

UC Riverside Electronic Theses and Dissertations

Title

Synthesis and Computational Binding Studies of Cannabinoid Analogues; Simple Computational Methods of Predicting Asymmetric Reactions

Permalink

<https://escholarship.org/uc/item/5kb8s3tw>

Author

Gutierrez, Michael

Publication Date

2013

Peer reviewed|Thesis/dissertation

UNIVERSITY OF CALIFORNIA
RIVERSIDE

Synthesis and Computational Binding Studies of Cannabinoid Analogues; Simple
Computational Methods of Predicting Asymmetric Reactions

A Dissertation submitted in partial satisfaction
of the requirements for the degree of

Doctor of Philosophy

in

Chemistry

by

Michael Scott Gutierrez

August 2013

Dissertation Committee:

Dr. Michael J. Marsella, Chairperson

Dr. Thomas H. Morton

Dr. Robert C. Haddon

Copyright by
Michael Scott Gutierrez
2013

The Dissertation of Michael Scott Gutierrez is approved:

Committee Chairperson

University of California, Riverside

Acknowledgements

To Prof. Michael Marsella: I can't thank you enough for your guidance, knowledge, and understanding these past years. I know that what you have instilled in me will not be forgotten, and I hope that I will be able to pass along all that I have learned from you to others that I teach.

I would like to thank my committee members, Prof. Thomas Morton and Prof. Robert Haddon for reviewing my dissertation. I would also like to thank Prof. Christopher Switzer for acting as a proxy and sitting in on three defenses in one day in addition to reviewing my dissertation.

Many thanks to: Bobby Carp for your friendship and help these past years; Bobby Bastin for your help with the Δ^6 -THC project; Mackenzie Alvarez for your help with various projects as both an undergrad and a grad student in our group.

To my wife, Cynthia and daughter, Elliana: Thank you for not letting me give up and giving me a reason to press on.

To my Lord and Savior, Jesus Christ: I can do all things through You who gives me strength.

This dissertation is dedicated to my wife, Cynthia, and my daughter, Elliana. Thank you for your love and support and for putting up with me during the crazy times. I love you with all my heart. To my parents, John and Tammi Carlberg, thank you for always being there for me and standing behind me in everything I've chosen to do. Finally, to the memory of Dr. Wayne Fritch, if not for his high school chemistry class, I probably would have become a lawyer.

ABSTRACT OF THE DISSERTATION

Synthesis and Computational Binding Studies of Cannabinoid Analogues; Simple
Computational Methods of Predicting Asymmetric Reactions

by

Michael Scott Gutierrez

Doctor of Philosophy, Graduate Program in Chemistry
University of California, Riverside, August 2013
Prof. Michael J. Marsella, Chairperson

With the increased interest in the great therapeutic potential of cannabinoids also comes the need in finding more efficient methods for the facile synthesis of these compounds.

While most synthetic methodologies for the phytocannabinoids involve olivetol in some way, the synthetic pathways presented in this thesis utilize nonaromatic olivetol precursors in conjunction with a tandem Knoevenagel/Diels-Alder or Knoevenagel/oxo-6pi-cyclization to provide access to both natural and unnatural cannabinoids.

These compounds as well as analogues that could potentially be made by the methods provided in this thesis were also computationally screened for their affinity for the CB₁ receptor. In addition to this *in silico* screening, one particular analogue was biologically screened and preliminary studies demonstrated a therapeutic potential towards ALS.

The second project presented in this thesis describes a computationally inexpensive, yet highly accurate, method towards predicting the asymmetric induction of certain reactions. This method examines the electrostatic potential mapped onto the surface of a molecule at the reactive site and at the same time allows for the examination of sterics, if applicable.

Table of Contents

Chapter One	Synthetic Evolution and Pharmacotherapy of Delta-1-Tetrahydrocannabinol and other Cannabinoids	1
1.1	History and Classification of the Cannabinoids	2
1.2	Synthetic Evolution of Δ^1 -THC	5
1.2.1	Biosynthetic Pathway of Cannabinoids	5
1.2.1	Early Synthetic Attempts towards Δ^1 -THC	7
1.2.2	First Asymmetric Synthesis of Δ^1 -THC	9
1.2.3	First Asymmetric Synthesis of R,R- Δ^1 -THC	11
1.3	Pharmacology and Pharmacotherapy of Cannabinoids	14
1.3.1	Discovery of the Cannabinoid Receptors	14
1.3.2	Mechanism of Cannabinoid Action	16
1.3.3	Cannabinoids as a Therapeutic Target for Pain and Inflammation	16
1.3.4	Cannabinoids as an Antiemetic	17
1.3.5	Cannabinoids as a Source of Symptomatic Treatment for Multiple Sclerosis	20
1.3.7	Targeting the Endocannabinoid System for Curative Cancer Therapies	21
	References	23
Chapter Two	Synthetic Pathways Towards Cannabinoid Analogues	27
2.1	Introduction	28
2.2	Facile Synthesis of Cannabinoid Analogues	28
2.2.1	The Use of Nonaromatic Olivetol Precursors Towards Δ^1 -THC and Analogues	26
2.2.2	Synthesis of Perhydro- and Tetrahydro- Cannabinoid Analogues	30
2.2.3	Revisiting Citral	34
2.3	The Pharmacological Potential of Δ^6 -THC	42
2.4	Synthesis of Other Cannabinoid Analogues	44
2.5	Summary	46
	References	47

Chapter Three	Computational and Biological Screening of Cannabinoid Analogues	48
3.1	Computational Binding Studies of Various Cannabinoids	49
3.1.1	Introduction	49
3.1.2	Protocol for Obtaining Binding Data	49
3.1.3	Binding Studies of Known Cannabinoid Ligands	50
3.1.4	Binding Studies of Unnatural Stereoisomers of Δ^1 - and Δ^6 -THC	52
3.1.5	Binding Studies of Methoxy Analogues of “ Δ^0 -THC”	53
3.1.6	Binding Studies of “Minimal” THC and Derivatives	54
3.2	Biological Screening of “Minimal” THC	57
3.3	Summary	59
	References	60
Chapter Four	Simple Computational Methods of Predicting Asymmetric Reactions	61
4.1	Introduction	62
4.2	Electrostatic Potential on LUMO surfaces (ESP@LUMO)	62
4.3	The Use of ESP at a Reactive Site (ESP@LUMO) to Examine Both Steric and Electronic Effects	64
4.4	Reduction of Asymmetric Carbonyls	65
4.5	Silacyclopropanations	69
4.6	Aldol Reactions	71
4.7	Reactions of Chiral Enolates with Prochiral Aldehydes	73
4.8	Summary	76
	References	78
Appendix A:	Experimental Procedures and Spectroscopic Data	81
Appendix B:	Atomic Coordinates of Compounds Found in Chapter 4	90

List of Figures

Figure 1.1. Structure and numbering system of (-)- Δ^1 -THC and (-)- Δ^9 -THC. The former structure represents the monoterpene numbering and the latter structure represents the formal numbering. The stereochemistry at the 3 and 4 carbons (10a and 6a) is R, R.

Figure 1.2. Structure of levonantradol.

Figure 2.1. Advantages for utilizing non-olivetol sources in the synthesis of aromatic and non-aromatic cannabinoids.

Figure 2.2. Computational results showing stereochemical control by enantiopure citronellal

Figure 2.3. Possible outcomes (indicated in blue) for the free radical bromination of hexahydrocannabinol.

Figure 2.4. Spartan calculations (B3LYP/6-31G*) performed by Angie Garcia for the starting materials, products, and transition states for the isomerization of non-aromatic and aromatic analogues of CBC.

Figure 2.5. Structures of (-)- Δ^1 -THC and cannabidiol (CBD).

Figure 3.1. (-)- Δ^1 -THC docked into a modeled CB1 receptor. The receptor is represented by the green ribbon.

Figure 3.2. The interaction of the four stereoisomers of “minimal THC” with the Thr197, Tyr275, Trp279, and Met363 residues.

Figure 3.3. ALS macrophages treated with stimulated superoxide dismutase 1 (SOD-1). **a)** negative control (not treated with SOD-1); **b)** positive control (treated with SOD-1); **c)** treated with SOD-1 then cannabichromene analog.

Figure 4.1. The ESP@LUMO map on fluoradamantone.

Figure 4.2. Comparison of ESP@RS method with ESP@LUMO method.

Figure 4.3. ESP@RS map on fluoradamantone.

Figure 4.4. Prediction of silacyclopropanation reactions of chiral alkenes using ESP@RS methodology. The alkene has the role of the nucleophile and the more electronegative face (more red) should yield the major product.

List of Schemes

- Scheme 1.1.** Proposed biogenetic pathway for Δ^1 -THC
- Scheme 1.2.** Mechoulam synthesis of (\pm) - Δ^1 -THC
- Scheme 1.3.** Taylor synthesis and Mechoulam modification towards (\pm) - Δ^1 -THC and isomers
- Scheme 1.4.** Fahrenholtz synthesis of (\pm) - Δ^1 -THC
- Scheme 1.5.** Evans retrosynthesis of Δ^1 -THC
- Scheme 1.6.** Synthesis of cycloadduct using a chiral bis(oxazoline) catalyst
- Scheme 1.7.** Evans synthesis of S,S- Δ^1 -THC
- Scheme 1.8.** Trost's retrosynthetic analysis of R,R- Δ^1 -THC.
- Scheme 1.9.** Synthesis of carbonate **5**.
- Scheme 1.10.** Mo-catalyzed asymmetric allylic alkylation reaction.
- Scheme 1.11.** Attempts at alkylating malonate **4** and monoester **12**.
- Scheme 1.12.** Final steps in the asymmetric synthesis of R,R- Δ^1 -THC.
- Scheme 2.1.** Retrosynthetic analysis utilizing a non-aromatic olivetol precursor.
- Scheme 2.2.** Synthesis of non-aromatic olivetol precursor.
- Scheme 2.3.** Knoevenagel-oxo- 6π electrocyclization reaction of citral with olivetol precursor.
- Scheme 2.4.** Synthesis of " Δ^0 -THC" **9** and its anisole derivative **10**.
- Scheme 2.5.** Transition state of stereochemically governed Diels Alder reaction
- Scheme 2.6.** Protection of citral.
- Scheme 2.7.** Use of protected citral towards THC analogues.
- Scheme 2.8.** Formation of sulfone **17**.

Scheme 2.9. Synthesis of CBC-Me.

Scheme 2.10. Synthesis of Δ^6 -THC-Me and potential isomerization to Δ^1 -THC-Me

Scheme 2.11. Possible mechanistic pathway for the formation of the methyl analogue of Δ^6 -THC in which citral undergoes an acid catalyzed cyclization followed by an electrophilic aromatic substitution.

Scheme 2.12. Alternative mechanistic pathway for the formation of the methyl analogue of Δ^6 -THC in which the electrophilic aromatic substitution occurs first followed by cyclization.

Scheme 2.13. Possible synthesis for a Δ^6 analog of Sativex™

Scheme 2.14. Synthesis of “minimal” THC

Scheme 2.15. The use of aldol condensations to functionalize “minimal” THC

Scheme 3.1. Possible pathways into “minimal” THC derivatives.

Scheme 4.1. Possible transition state conformations and products in the Aldol reaction between a prochiral aldehyde and chiral enolate.

List of Tables

Table 1.1. Examples of endo-, natural, and synthetic cannabinoids.

Table 1.2. 5-HT₃ receptor agonists used as antiemetics

Table 2.1. ¹³C-NMR data for the comparison of experimental results to a reference set.

Table 3.1. Results of computational binding studies of phyto- and synthetic cannabinoids.

Table 3.2. Results of computational binding studies of the unnatural stereoisomers of Δ^1 - and Δ^6 -THC.

Table 3.3. Results of computational binding studies of the trans isomers of the methoxy analogues of " Δ^0 -THC."

Table 3.4. Results of computational binding studies of "minimal" THC and derivatives.

Table 4.1. Results of predicting asymmetric reductions using ESP@RS methodology. ESP values are given at cross-hair points on each face of ketone carbon. ESP maps are shown for major and minor product faces in columns 2 and 3 respectively.

Table 4.2. Summary of results in the prediction of silacyclopropanation reactions. ESP values are given at the center of the alkene for each face.

Table 4.3. Summary of ESP@RS prediction results for the aldol reaction. The face which has the more positive electrostatic potential value at the cross-hairs is that which should be favored electrostatically. Sterics implies that one face or the other of the aldehyde was blocked from participating in the aldol reaction. (+) indicates that the prediction was correct, while (-) indicates that the prediction did not match experimental results.

Table 4.4. Summary of results in predicting the aldol reaction between 2-methylpropanal and chiral enolates containing amides. The predicted attacking face is that which has the more electronegative value.

Table 4.5. Summary of results in predicting the aldol reaction between prochiral aldehydes and chiral enolates. The predicted attacking face is that which has the more electronegative value.

Chapter One

Synthetic Evolution and Pharmacotherapy of Delta-1-Tetrahydrocannabinol and other Cannabinoids

1.1 History and Classification of the Cannabinoids

Cannabis Sativa is hypothesized to be known in Neolithic China around 4000 BC,¹ but its properties and therapeutic uses were not documented until 2737 BC² by the emperor of China, Shen Nung. After its spread to India from China, cannabis was found to have analgesic, appetite stimulant, antiemetic, muscle relaxant, and anticonvulsant properties.³ Cannabis was listed in the United States Dispensatory in 1854,⁴ and remained there until 1942 when it was removed from the United States Pharmacopoeia, thereby losing its legitimacy as a therapeutic agent.⁵

The isolation of Δ^1 -tetrahydrocannabinol (Δ^1 -THC, also known as Δ^9 -THC) from *Cannabis Sativa* in 1964⁶ has since sparked much synthetic study and, more recently, intense pharmacological examination. As one of more than sixty cannabinoids found in cannabis, (-)- Δ^1 -THC (Figure 1.1) is responsible for not only the notorious psychoactivity of cannabis, but its therapeutic effects as well. The discovery of the cannabinoid receptors CB₁⁷ and CB₂⁸ and Δ^1 -THC analogues that selectively bind to those receptors have necessitated the need for a flexible synthetic pathway with high yields and stereoselectivity.

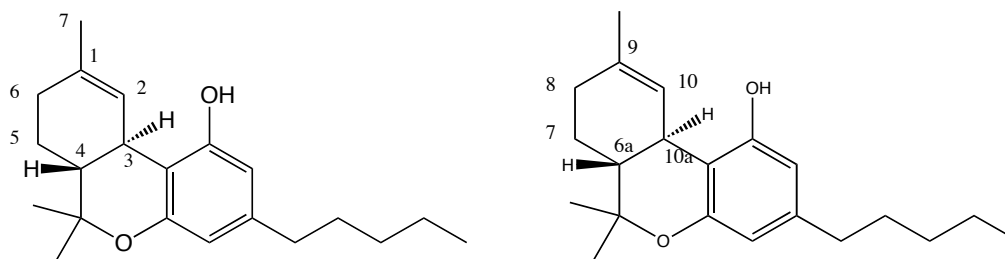


Figure 1.1. Structure and numbering system of (-)- Δ^1 -THC and (-)- Δ^9 -THC. The former structure represents the monoterpenoid numbering and the latter structure represents the formal numbering. The stereochemistry at the 3 and 4 carbons (10a and 6a) is R, R.

Cannabinoids can be grouped into three classes: endogenous (naturally occurring cannabinoids found in the body), natural (those found in the plant specie *Cannabis*), and synthetic. Endogenous cannabinoids, also known as eicosanoids, include anandamide, 2-arachidonoyl glycerol ether, 2-arachidonoyl glycerol (2-AG), N-arachidonoyl-dopamine (NADA) and virodhamine. The natural cannabinoids are similar in structure yet do not all share the same bioactivity. In addition to Δ^1 -THC, these include delta-6 tetrahydrocannabinol (Δ^6 -THC), cannabiol (CBN), cannabicyclol (CBL), cannabigerol (CBG), and cannabichromene (CBC). These compounds have no significant psychotropic effects compared to Δ^1 -THC,⁹ however, they may have an impact on the effects of Δ^1 -THC.¹⁰ Synthetic cannabinoids include dronabinol (Marinol), levonantrodol, nabilone, HU-210, CP-55,940, and WIN-55,212-2. It should be noted that some synthetic cannabinoids do not adhere to the typical structure found in the natural cannabinoids (See Table 1.1).

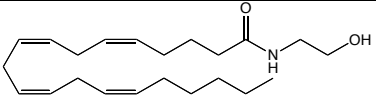
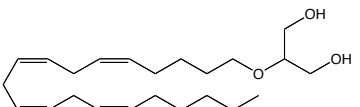
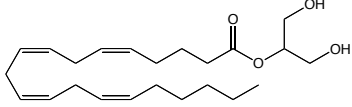
<u>Class</u>	<u>Name</u>	<u>Structure</u>
<i>Endocannabinoid</i>	Anandamide	
	2-arachidonoyl glycerol ether	
	2-arachidonoyl glycerol	

Table 1.1. Examples of endo-, natural, and synthetic cannabinoids.

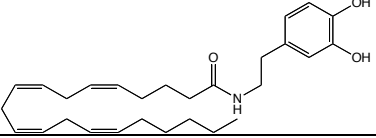
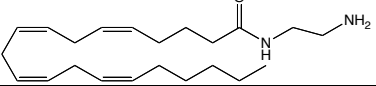
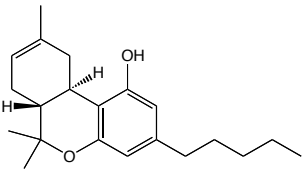
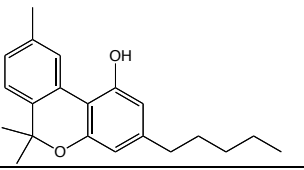
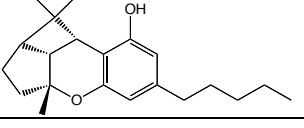
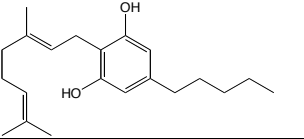
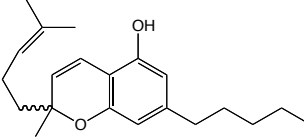
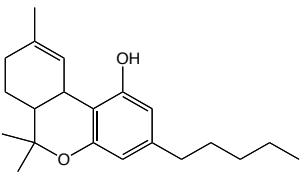
<u>Class</u>	<u>Name</u>	<u>Structure</u>
<i>Endocannabinoid (Continued)</i>	N-arachidonoyl-dopamine	
	Virodhamine	
<i>Natural</i>	Delta-6 tetrahydrocannabinol	
	Cannabinol	
	Cannabicyclol	
	Cannabigerol	
	Cannabichromene	
<i>Synthetic</i>	Dronabinol	 <i>Racemic mixture of (+)-Δ¹-THC</i>

Table 1.1. Continued

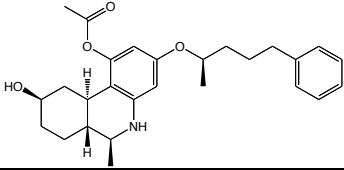
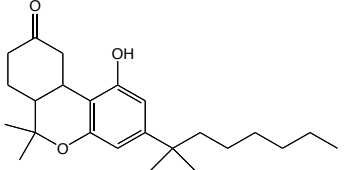
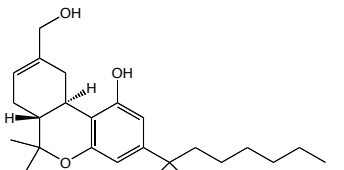
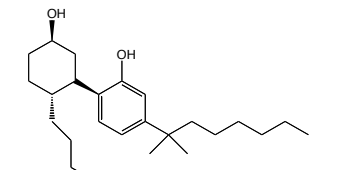
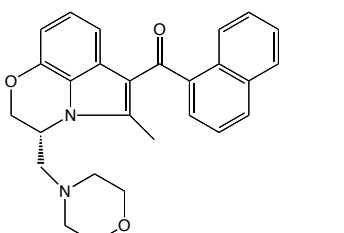
<u>Class</u>	<u>Name</u>	<u>Strucutre</u>
<i>Synthetic (Continued)</i>	Levonantradol	
	Nabilone	 <i>Racemic mixture of R,R and S,S isomers</i>
	HU-210	
	CP-55,940	
	WIN-55,212-2	

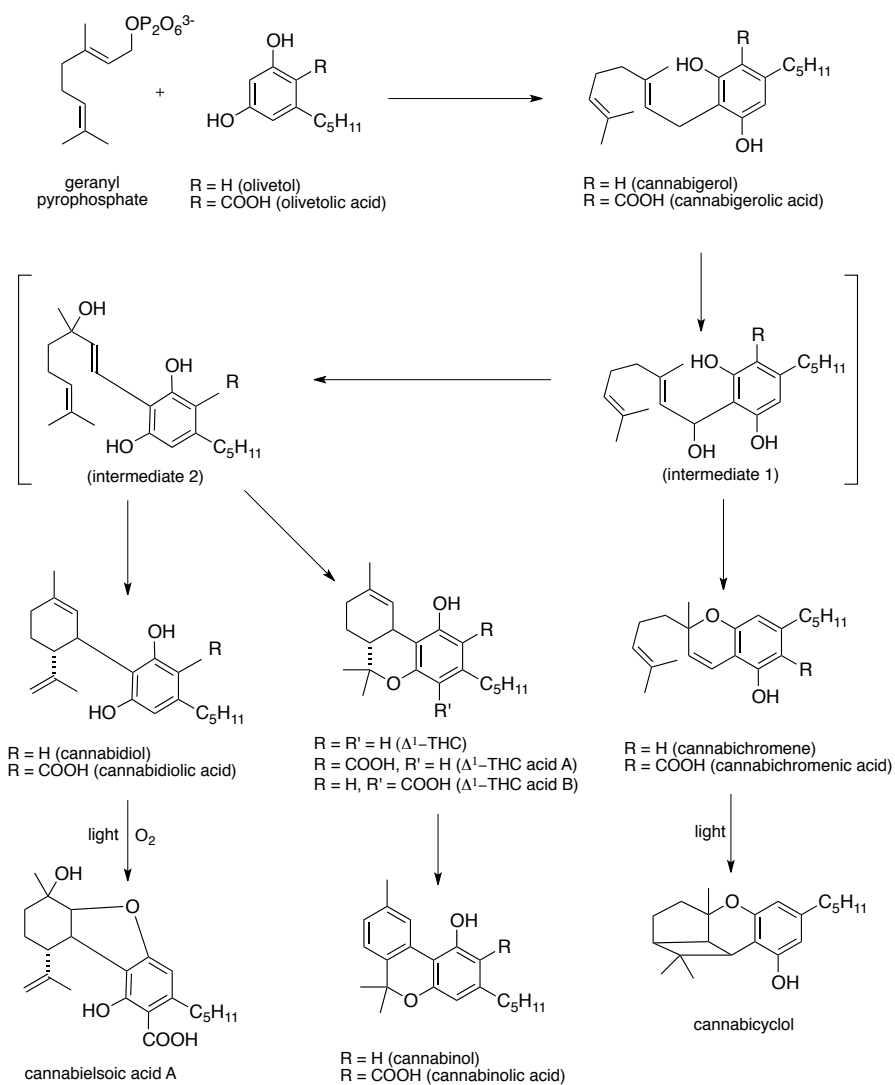
Table 1.1. Continued

1.2 Synthetic Evolution of Δ^1 -THC

1.2.1 Biosynthetic Pathway of Cannabinoids

While the actual biosynthetic pathway for the formation of cannabinoids is still under study, Scheme 1.1 gives a good idea for this process.¹² This scheme proposes that

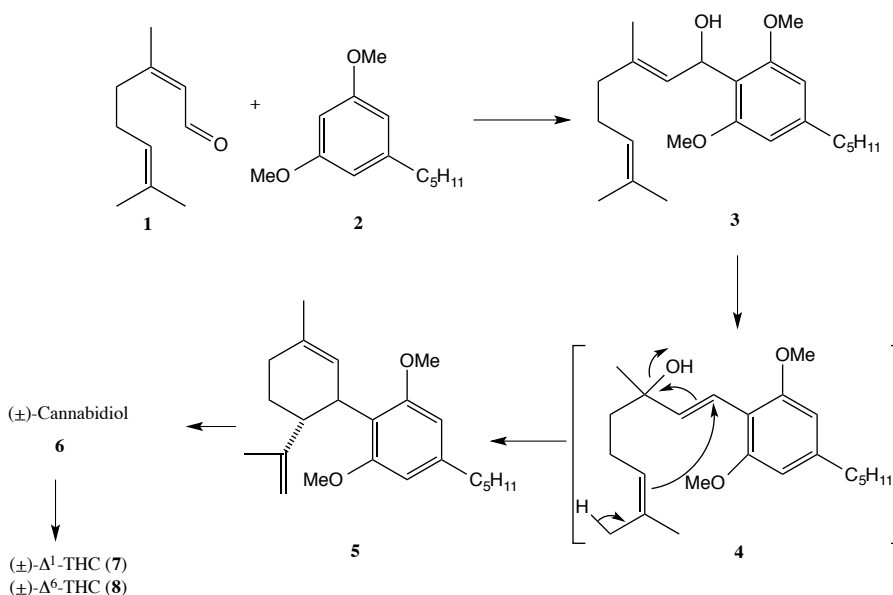
geranyl pyrophosphate and olivetolic acid form cannabigerolic acid. Following an allylic rearrangement from **intermediate 1** to **intermediate 2** to yield cannabidiolic acid, cannabielsoic acid A then forms after exposure to light and oxygen. Δ^1 -THC acid A can be directly obtained from cannabigerolic acid via an enzymatic oxidation-cyclization process.¹³ Cannabichromenic acid can be obtained from the proposed intermediate 1 which in turn can yield cannabicyclol.¹⁴



Scheme 1.1. Proposed biogenetic pathway for Δ^1 -THC

1.2.2 Early Synthetic Attempts towards Δ^1 -THC

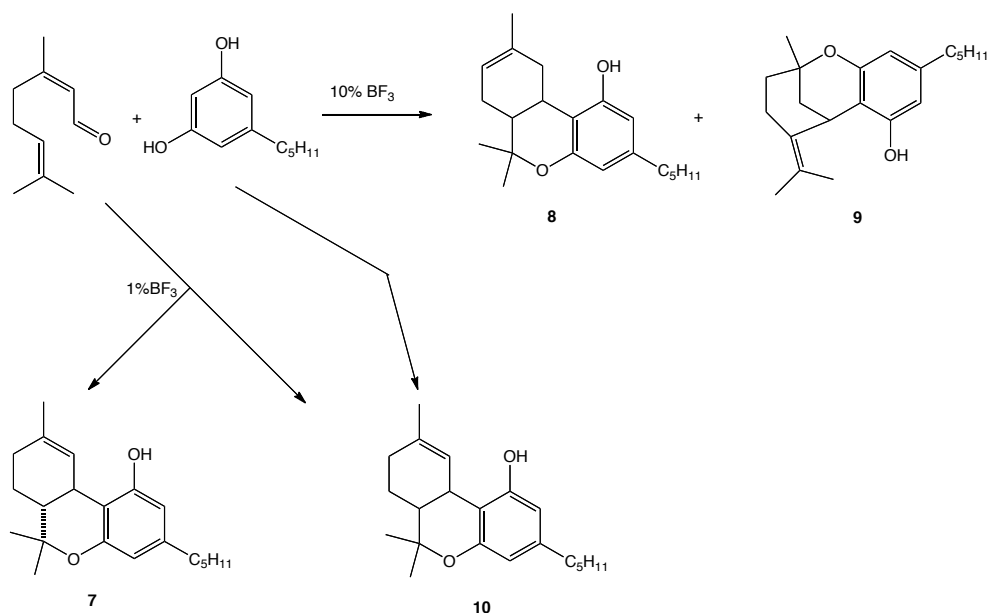
The first successful attempt at the synthesis of Δ^1 -THC was first reported by Gaoni and Mechoulam a year after they isolated the compound from plant material.¹⁵ Patterned after the proposed biogenetic pathway (Scheme 1.1), citral was utilized (as opposed to geraniol) with the lithium derivative of olivetol dimethyl ether to afford a mixture thought to contain **3**. (\pm)-Dimethyl cannabidiol **5** was obtained after tosylation through a proposed allylic rearrangement **4**. **5** was demethylated at high temperatures with methylmagnesium iodide resulting in (\pm)-cannabidiol (**6**) and was subsequently converted to a mixture of (\pm)- Δ^1 -THC (**7**) and (\pm)- Δ^6 -THC (**8**) by acid treatment (Scheme 1.2). The overall yield for the synthesis was only 2%.



Scheme 1.2. Mechoulam synthesis of (\pm)- Δ^1 -THC

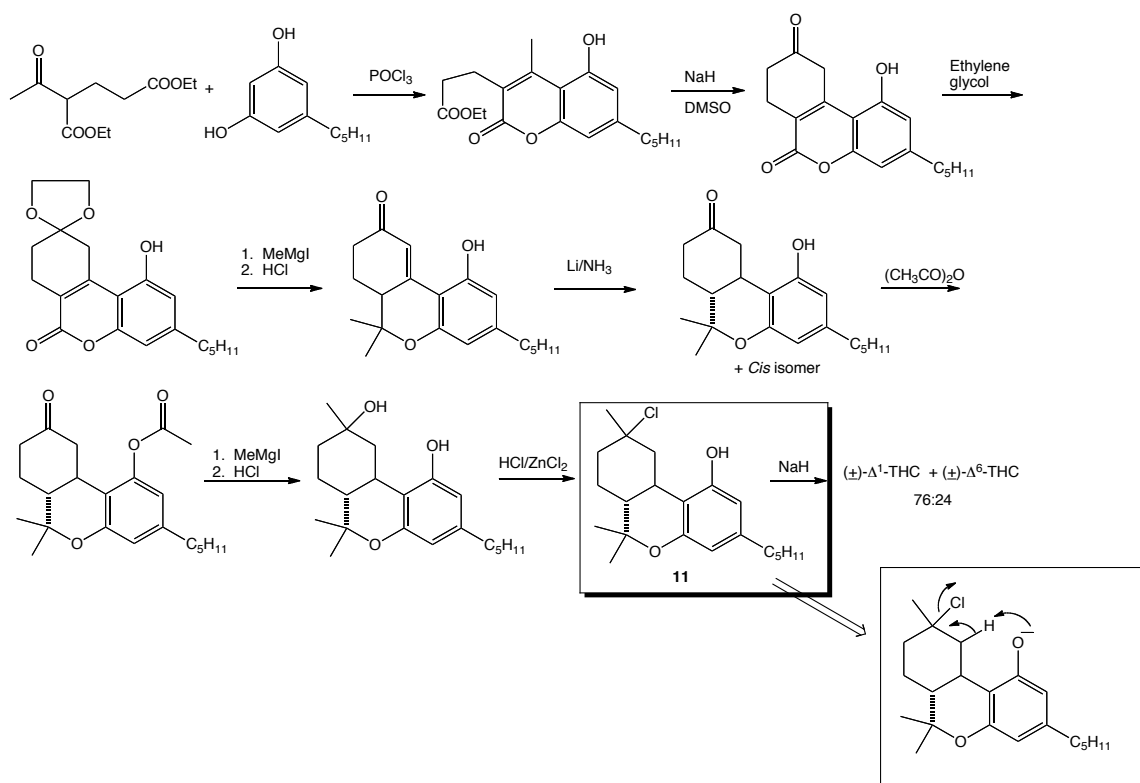
Taylor and coworkers shortly thereafter reported a one-step synthesis¹⁶ using citral and olivetol in 10% BF_3 to give (\pm)- Δ^6 -THC (**8**) in 10-20% yield and another

compound later to be identified as the isocannabinoid (**9**). By using hydrochloric acid in ethanol, Taylor was able to obtain previously unsynthesized (+)-*cis*- Δ^1 -THC (**10**) in 20% yield along with a small amount of the trans isomer, however was unable to separate the two isomers. Mechoulam and coworkers were able to later modify Taylor's synthesis by using 1% BF_3 in methylene chloride to give (+)-*trans*- Δ^1 -THC (**7**) in a 20% yield along with (+)-*cis*- Δ^1 -THC (**10**).¹⁷ Scheme 1.3 summarizes these reactions.



Scheme 1.3. Taylor synthesis and Mechoulam modification towards (+)- Δ^1 -THC and isomers

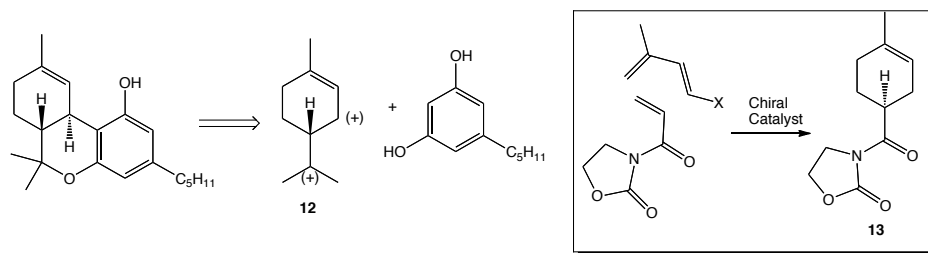
Fahrenholtz and coworkers reported an original synthesis of racemic Δ^1 -THC and Δ^6 -THC (and subsequently four of its isomers) in 1967.¹⁸ Scheme 1.4 outlines their synthetic pathway but of most interest is the reaction of compound **11** with sodium hydride to yield a 76:24 mixture of Δ^1 -THC: Δ^6 -THC. It is believed that the regioselectivity of this reaction is due to the formation of the phenolate ion and subsequent internal dehydrohalogenation (See inset of Scheme 1.4).



Scheme 1.4. Fahrenholtz synthesis of (±)- Δ^1 -THC

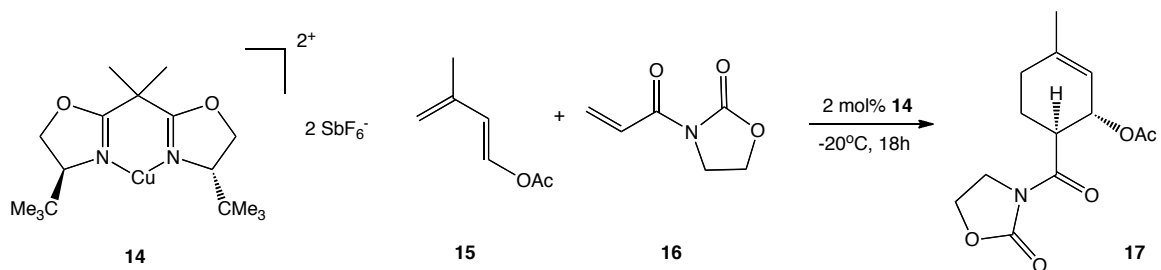
1.2.3 First Asymmetric Synthesis of Δ^1 -THC

In 1997, David Evans and coworkers reported the first asymmetric synthesis of *S,S*- Δ^1 -THC using a bis(oxazoline)Cu(II) complex catalyzed Diels-Alder reaction as the key step for the asymmetric induction.¹⁹ Inspired by previous synthetic routes involving the use of monoterpenes that function as a hypothetical dication synthon **12** (Scheme 1.5), the Evans group sought to create a chiral cycloadduct **13** from achiral starting materials to serve as their dication synthon.



Scheme 1.5. Evans retrosynthesis of Δ^1 -THC

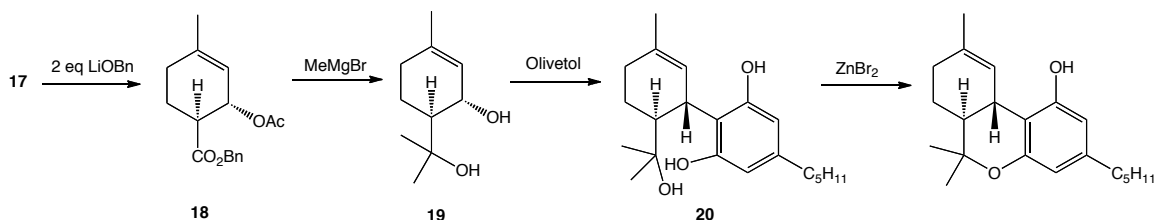
The Diels-Alder reaction of diene **15** and acrylimide **16** using the copper(II) complex catalyst **14** gave the cycloadduct **17** in a 57% yield with a 73:27 (*exo*:*endo*) mixture of diastereomers with the major stereoisomer formed with 98% ee (Scheme 1.6). This was unexpected as a test reaction with 1-acetoxybutadiene underwent the cycloaddition with a high *endo* selectivity. It was hypothesized that the steric interaction between the ligand and the methyl group of **15** accounts for the shift in diastereoselectivity to the *exo* product.



Scheme 1.6. Synthesis of cycloadduct using a chiral bis(oxazoline) catalyst

Imide **17** was selectively cleaved using LiOBn followed by the formation of diol **19** with six equivalents of methylmagnesium bromide. This diol was then condensed onto olivetol to afford cannabidiol analog **20**. The final cyclization was performed using ZnBr_2 (Scheme 1.7). Contamination from isomeric THC-related products were not

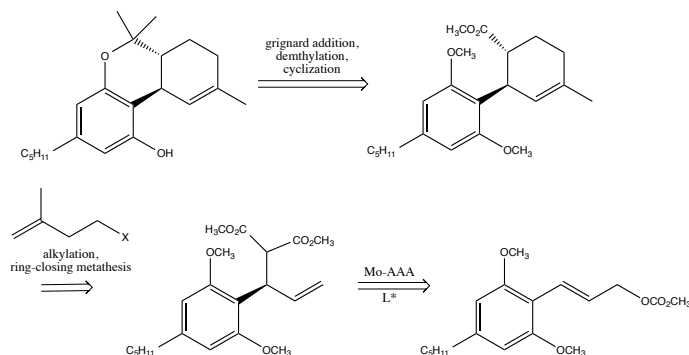
observed, contrary to other synthetic attempts at Δ^1 -THC. This synthesis was accomplished with an 21% yield overall.



Scheme 1.7. Evans synthesis of S,S - Δ^1 -THC

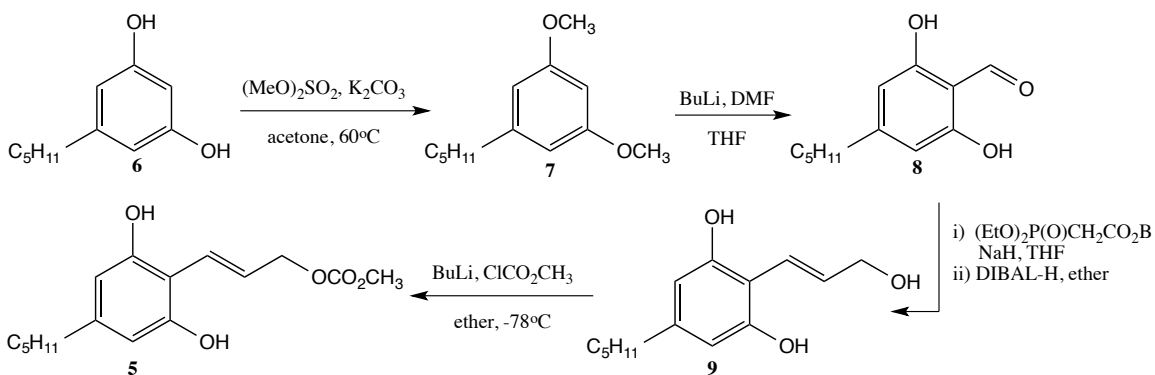
1.2.4 First Asymmetric Synthesis of R,R - Δ^1 -THC

While the Evans synthesis of THC was the first example of a stereospecific route to a THC isomer, synthesis of the actual stereoisomer found in cannabis (R,R - Δ^1 -THC) was not reported until 2007 by Barry Trost and Kalindi Dogra.²⁰ Trost's retrosynthetic analysis includes setting all of the stereochemistry from a single Mo-catalyzed asymmetric allylic alkylation reaction (Scheme 1.8). This synthetic route could also allow access to other analogues of THC by varying the aromatic group in **5**, the alkylating partner **3**, or the Grignard reagents.



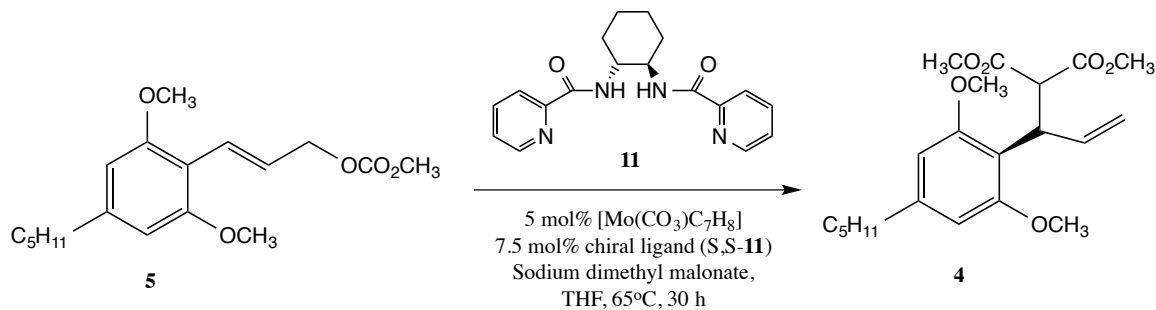
Scheme 1.8. Trost's retrosynthetic analysis of R,R - Δ^1 -THC.

Scheme 1.9 below outlines the synthesis of carbonate **5**. The final step for this fragment proved to be somewhat difficult. This compound was very sensitive to both acid and base, including silica chromatography methods. Therefore a preparation had to be devised to allow for the isolation of **5** but include satisfactory purification so that a clean reagent could be carried on to the Mo-alkylation reaction. This was achieved by titrating alcohol **9** with BuLi at -78°C and quenching the alkoxide with methyl chloroformate, also at -78°C . The resulting organic layer was washed with ice-cold water to give a stable solid.



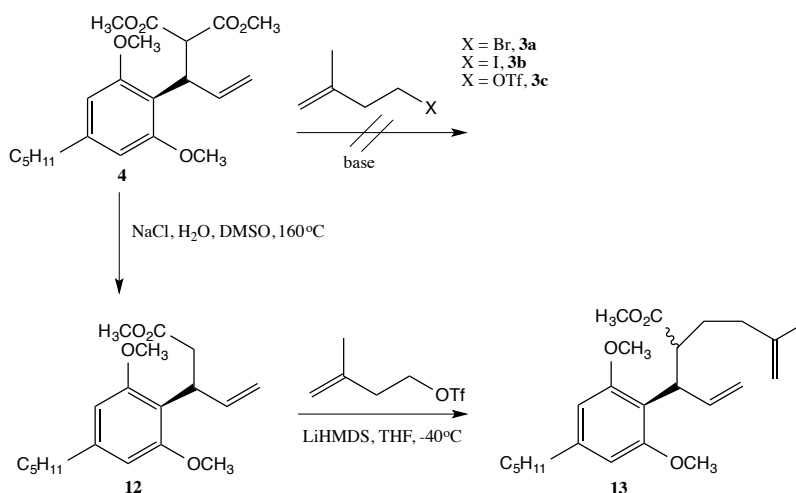
Scheme 1.9. Synthesis of carbonate **5**.

Concern was given to the steric interference of the *o*-methoxy groups in hindering the Mo-alkylation reaction. However, this was not observed and compound **4** was obtained (after optimization) in 95% yield with 94% ee (Scheme 1.10). Attempts to alkylate **4** were unsuccessful as steric congestion at the malonate carbon prevented any



Scheme 1.10. Mo-catalyzed asymmetric allylic alkylation reaction.

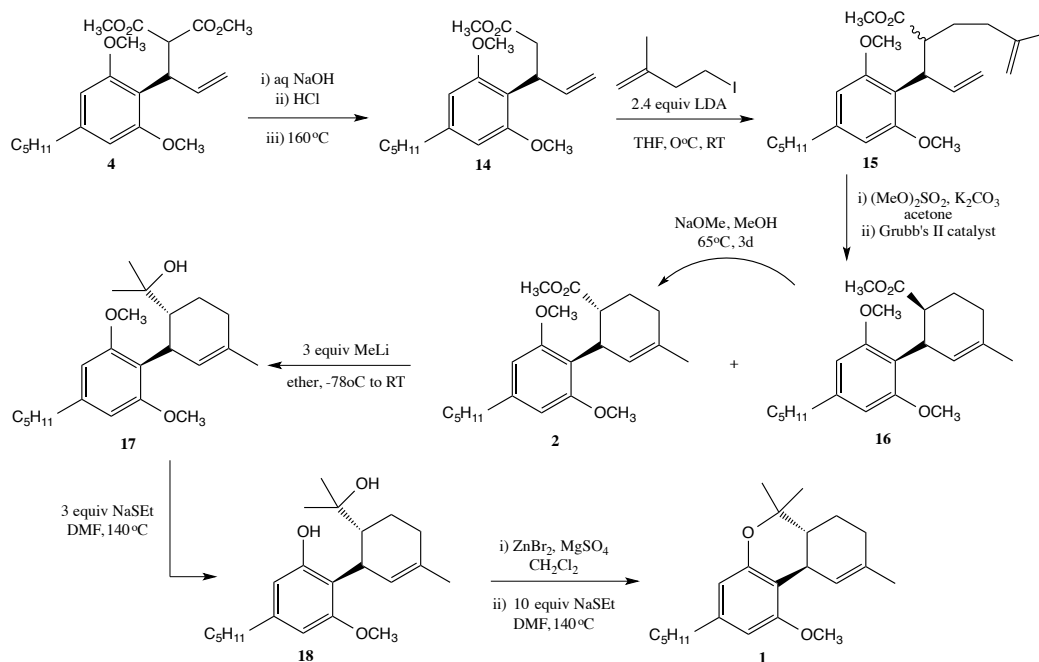
alkylation (even when tested with MeI as the alkylating agent). An alternate pathway was then devised using monoester **12** to reduce the steric demands (Scheme 1.11). These



Scheme 1.11. Attempts at alkylating malonate **4** and monoester **12**.

reactions had to be performed at low temperatures to avoid the instability of the enolates of methyl esters above -35°C . The low yields as well as the competing elimination reaction of the alkylating reagent caused the author to seek a nucleophile whose enolate was stable at room temperature or higher. The answer to this problem was found in the dianion of acid **14**. Scheme 1.12 outlines the successful use of this compound and its

subsequent utilization for the synthesis of R,R- Δ^1 -THC in 12 steps with a 31% overall yield.



Scheme 1.12. Final steps in the asymmetric synthesis of R,R- Δ^1 -THC.

1.3 Pharmacology and Pharmacotherapy of Cannabinoids

1.3.1 Discovery of the Cannabinoid Receptors

Drug-receptor interactions were first demonstrated by L.E. Hollister and G. Jones in separate studies in 1974. Strict structural selectivity²¹ as well as stereoselectivity²² were discovered after the studies of the biological effects of THC and some synthetic analogs. Further evidence for the existence of a specific cannabinoid receptor was presented by W. Devane and coworkers by the demonstration of high-affinity, saturable,

sterospecific binding sites for the synthetic cannabinoid agonist [3H]CP-55,940 (See Table 1.1 for structure) in mouse brain plasma membranes.²³ Radiological mapping of the cannabinoid receptors in the brain²⁴ led to the subsequent identification and cloning of an orphan G protein-coupled receptor (GPCR) as the brain receptor for cannabinoids,²⁵ later named CB₁ receptor. CB₁ receptors are most concentrated in the cerebellum, hippocampus and basal ganglia.²⁶ A second cannabinoid GPCR, CB₂, was identified and cloned by S. Munro²⁷ and was found to be expressed primarily in cells of the immune and hematopoietic systems. However, more recently, the CB₂ receptor were found to be present in the brain,²⁸ in nonparenchymal cells of cirrhotic liver,²⁹ in the endocrine pancreas,³⁰ and in bone.³¹

One important role of the CB₁ component of the endocannabinoid system is to modulate neurotransmitter release so that a homeostasis in health and disease is maintained by preventing excessive neuronal activity from developing in the central nervous system.³² This is evidenced by the following: (1) neuronal CB₁ receptors are located mainly at the terminals of central and peripheral neurons; (2) these receptors can mediate inhibition of ongoing release of many excitatory and inhibitory transmitters such as acetylcholine, noradrenaline, dopamine, 5-hydroxytryptamine, γ -aminobutyric acid, glutamate, D-aspartate, and cholecystokinin;³³⁻³⁵ and (3) endocannabinoids serve as retrograde synaptic messengers.³⁶

1.3.2 Mechanism of Cannabinoid Action

Before specific receptors were discovered, it was known that cannabinoids inhibit adenylyl cyclase (AC) resulting in a decrease in intracellular cAMP levels.³⁷ Further examination has revealed various signal transduction pathways involved with these compounds. As stated previously, cannabinoids act upon their specific receptors, CB₁ and CB₂, which are coupled to AC through heterotrimeric G_{i/o} proteins.³⁸ The CB₁ receptor modulates ion channels, inhibiting N- and P/Q-type voltage-sensitive Ca²⁺ (VSCC) and activating rectifying K⁺ channels.³⁹ Cannabinoid receptors are also coupled to activation of extracellular signal-regulated kinase (ERK),⁴⁰ c-Jun N-terminal kinase,⁴¹ and p38 mitogen-activated protein kinase,⁴² and protein kinase B (PKB).⁴³ Cannabinoids adjust sphingolipid-metabolizing pathways by inducing gomyelin breakdown and increase the levels of the second messenger ceramide.⁴⁴ Similar coupling between a plasma membrane receptor and neutral sphingomyelinase has been described for the 55-kDa tumor necrosis factor receptor.⁴⁵

1.3.3 Cannabinoids as a Therapeutic Target for Pain and Inflammation

Historical documents have shown the use of cannabis in surgical anesthesia in ancient China and to relieve many types of pain in ancient Israel, Greece, Rome, and India.³ Anandamide, THC, CBD, and synthetic cannabinoids such as CP55,940 and WIN 55,212-2 are effective against chemical,⁴⁶ mechanical,⁴⁶ and thermal pain stimuli.⁴⁷ Recently, anandamide and cannabinoid ligands were shown to be very effective against chronic neuropathic⁵⁸ and inflammatory pain.⁴⁹ When combined with commonly used

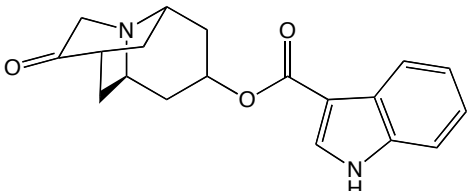
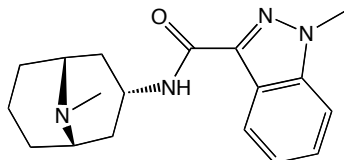
nonsteroid anti-inflammatory drugs, endo- and synthetic cannabinoids have demonstrated synergistic analgesic effects.⁴⁹

In two studies involving the smoking of cannabis for the treatment of HIV-associated neuropathy (resulting from HIV-infection or treatment) 46% to 52% of patients reported a greater than 30% reduction in pain.^{50,51} It was also reported that the cannabis treatment did not negatively impact the already compromised immune system. Dronabinol (See Table 1.1) is frequently used to counteract AIDS-related wasting and promote appetite in patients suffering from AIDS-related anorexia.⁵¹ Several cannabinoid-based medications have been examined as methods of pain treatments for multiple sclerosis (MS) patients. Dronabinol was shown in separate studies to reduce spontaneous pain intensity (over a 3 week treatment period), improve median radiating pain intensity and pressure threshold.⁵² Similar effects were observed in a study using Cannador®, a 2:1 ratio of Δ^1 -THC:CBD isolated from cannabis extract.⁵³ MS patients receiving Sativex® (cannabis extract containing a 1:1 ratio of Δ^1 -THC:CBD and administered as an oral-mucosal spray) reported a significant reduction in pain symptoms over a 4 week period.⁵⁴

1.3.4 Cannabinoids as an Antiemetic

A frequent adverse side effect of cancer chemotherapy is nausea and vomiting which can sometimes be severe and prolonged. While the most widely used antiemetics in the 1970s and 1980s included prochlorperazine, metoclopramide, and haloperidol, studies were conducted on evaluating the antiemetic effects of nabilone and dronabinol.

From 1979 to 1983, 15 controlled studies occurred with a total of 600 patients suffering from various cancers received nabilone and 14 controlled studies occurred with a total of 681 patients received dronabinol.⁵⁵ In all studies both nabilone and dronabinol were significantly superior to other antiemetic drugs. However, the effectiveness of these cannabinoid drugs were eclipsed by their high and often severe occurrence of undesirable side effects including drowsiness, euphoria, hallucinations, transient loss of emotional or physical control, hypotension, and sleep disorders.⁵⁵ Interest in dronabinol and nabilone decreased significantly with the advent of 5-HT₃ receptor antagonists such as dolasetron, granisetron, ondansetron, palonosetron and tropisetron (see Table 1.2).⁵⁵ These drugs are more potent, do not exhibit significant psychotropic effects and can be administered intravenously.

<u>Name</u>	<u>Trademark Name</u>	<u>Structure</u>
Dolasetron	Anzemet®	
Granisetron	Kytril®	

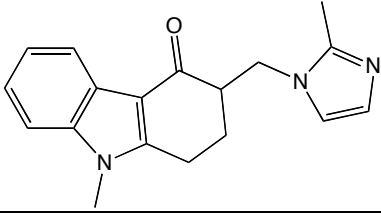
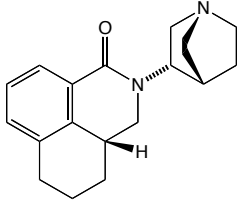
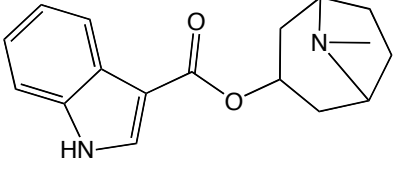
Ondansetron	Zofran®	
Palonosetron	Aloxi®	
Tropisetron	Navoban® or Setrovel®	

Table 1.2. 5-HT₃ receptor agonists used as antiemetics

In a study involving 108 patients levonantradol (see Figure 1.3), a synthetic cannabinoid administered intramuscularly, was found to be more effective than chlorpromazine as an antiemetic, however, its adverse side effects limited its utility.⁵⁶

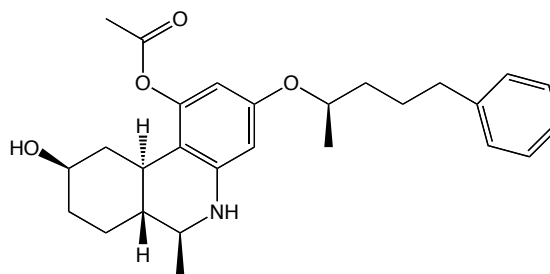


Figure 1.2. Structure of levonantradol

1.3.5 Cannabinoids as a Source of Symptomatic Treatment for Multiple Sclerosis

Multiple sclerosis (MS) is an inflammatory disease in which the fatty myelin sheaths around the axons of the brain and spinal cord are damaged, leading to demyelination and scarring as well as a broad range of signs and symptoms such as spasticity (muscle rigidity), sensitivity or tingling, pricking or numbness (hypoesthesia and paraesthesia), muscle weakness, muscle spasms, ataxia, problems in speech or swallowing, visual problems, fatigue, acute or chronic pain, and bladder or bowel difficulties.⁵⁷ Success of current symptomatic treatments are moderate at best and frequently result in adverse side effects ranging from flushing, chest tightness, heart palpitations, breathlessness and anxiety⁵⁷ to more serious side effects such as liver damage⁵⁸, severe cardiotoxicity, infertility, and acute myeloid leukaemia.⁵⁷ Subjective reports of patients self-medicating with cannabis suggest it may control some symptoms such as spasticity, tremor, and pain and bladder dysfunction.⁵⁷

In 2003 a study of 630 MS patients was performed in which 206 individuals received Marinol®, 211 patients received Cannador®, and 213 patients took a placebo.⁵³ Over the course of 14 weeks the authors reported the absence of positive effects on spasticity, however, objective improvement was reported in mobility with Marinol® and subjective improvement was reported in muscle spasms, pain, sleep quality and general condition, as well as a decrease in hospitalizations for relapses for both Marinol® and Cannador®.⁵³ A 1-year follow up of this study in which 80% of the patients participated

revealed an overall objective improvement in spasticity and general disability with only minor adverse effects reported in 361 of the patients.⁵³

1.3.6 Targeting the Endocannabinoid System for Curative Cancer Therapies

The previous sections were all examples utilizing cannabinoids for *symptomatic* treatment of various diseases and disorders. This current section outlines promising research involved in the curative treatment of cancer through the use of the endocannabinoid system.

Since mitogen- and stress-activated protein kinase cascades, PKB, and ceramide are widely accepted to be involved in the control of the fate of different cells, it is possible that cannabinoids may have a role in the decision of cell survival or death.³⁹ Cannabinoids have demonstrated the induction of cell death of tumor cells such as C6 glioma cells,⁶⁰ PC-12 pheochromocytoma cells,⁶¹ and hippocampal neurons⁶², *in vitro*, as well as cause regression of C6-cell gliomas *in vivo*.⁶³ In the last study, rats infected with malignant tumors that were treated with natural THC and WIN-55,212-2 survived significantly longer than the control rats, and 20-35% of the treated animals displayed complete eradication of the tumors. Since the effect was observed with both cannabinoid samples, the researchers suggested that the cannabinoid receptors were involved in the antiproliferative effect of these cannabinoids *in vivo*.⁶³ In addition, observations indicated that the treatment did not cause significant damage to surrounding healthy cells.

Di Marzo and coworkers have reported notable antiproliferation action on MCF-7, EFM-19, and T-47D (human breast cancer cells, HBCCs) using anandamide through a CB₁-mediated mechanism.^{64,65}

1. McKim, W.A. *Drugs and Behavior. An Introduction to Behavioral Pharmacology*, 4th ed. Prentice-Hall, Upper Saddle River, 2000.
2. Li, H.L. *Economic Botany*. **1974**, 28, 437.
3. Mechoulam, R. *Cannabinoids as Therapeutic Agents*. CRC Press, Boca Raton, 1986.
4. Robson, P. *British Journal of Psychiatry*. **2001**, 178, 107.
5. Fankhauser, M. *Cannabis and Cannabinoids: Pharmacology, Toxicology and Therapeutic Potential*. The Haworth Integrative Healing Press, New York, 2002.
6. Mechoulam, R.; Gaoni, Y. *J Amer Chem Soc*, **1964**, 86, 1646.
7. Matsuda LA, Lolait SJ, Brownstein MJ, Young AC, Bonner TI. *Nature* **1990**; 346, 561.
8. Munro S, Thomas KL, Abu-Shaar M. *Nature* **1993**; 365, 61.
9. Smith, P.F. *Current Opinion in Investigational Drugs*. **2004**, 5, 727.
10. Ashton, C.H. *British Journal of Psychiatry*. **2001**, 178, 101.
11. Mechoulam, R.; Gaoni, Y. *J Amer Chem Soc* **1965**, 87, 3273.
12. Mechoulam, R., *Current Pharmaceutical Design*, **2000**, 6, 1313-1322.
13. Taura, F.; Morimoto, S; Shoyama, Y.; Mechoulam, R., *J Amer Chem Soc*, **1995**, 117, 9766.
14. Mechoulam, R.; Gaoni, Y., *J Amer Chem Soc*, **1965**, 87, 3273-3275.
15. Mechoulam R. *Marijuana. Chemistry, Metabolism, Pharmacology and Clinical Effects*. Academic Press, New York, 1973.
16. Edward C. Taylor, Katherine Lenard, Youval Shvo. *J Amer Chem Soc*, **1966**, 88, 367.
17. Mechoulam, R.; Gaoni, Y. *J Amer Chem Soc*, **1972**, 94, 6159.
18. Fahrenholtz, K. E., Lurie, M., and Kierstead, R.W. *J Amer Chem Soc*, **1972**. 89, 5934.

19. Evans, D. A.; Shaughnessy, E. A.; Barnes, D. M. *Tetrahedron Letters* **1997**, *38*, 3193.
20. Trost, B. M.; Dogra, K. *Organic Letters* **2007**, *9*, 861.
21. Hollister L.E. *Pharmacology*. **1974**. *11*, 3.
22. Jones, G; et al. *Biochem Pharmacol*. **1974**. *23*, 439.
23. Devane, W.A.; et al. *Mol Pharmacol*. **1988**. *34*, 605.
24. Herkenham, M.; et al. *J Neurosci*. **1991**. *11*, 563.
25. Matsuda, L. A.; et al. *Nature (Lond)*. **1990**. *346*, 561.
26. L.S.; De Costa, B.R.; Rice, K.C. *Proceedings of the National Academy of Sciences of the United States of America*, **1990**, *87*, 1932.
27. Munro, S.; et al. *Nature (Lond)*. **1993**. *365*, 61.
28. Van Sickle, M.D.; et al. *Science*. **2005**. *310*, 329.
29. Julien, B.; et al. *Gastroenterology*. **2005**. *128*, 742.
30. Juan-Pico, P.; *Cell Calcium*. **2005**. *39*, 155.
31. Idris, A.I.; et al. *Nat Med*. **2005**. *11*, 774.
32. Pertwee, R.G. *Br J Pharmacol*. **2008**. *153*, 199.
33. Howlett A.C.; et al. *Pharmacol Rev*. **2002**. *54*, 161.
34. Pertwee, R.G., Ross, R.A., *Prostaglandins Leukot Essent Fatty Acids* **2002**, *66*, 101-121.
35. Szabo, B., Schlicker, E., *Cannabinoids. Handbook of Experimental Pharmacology*, Vol 168. Springer-Verlag: Heidelberg, pp. 327-365.
36. Kreitzer A.C., *Curr Biol*. **2005**. *15*, 549.
37. Howlett, A.C., *Life Sci.*, **1984**. *35*, 1803-1810.
38. Pertwee, R.G., *Pharmacol Ther.*, **1997**. *74*, 129-180.

39. Guzman, M., Sanchez, C., Galve-Roperh, I., *J Mol Med*, **2001**, 78, 613-625.
40. Wartmann, M., et. al., *FEBS Lett*, **1995**, 359, 133-136.
41. Liu, J., et. al., *Biochem J*, **2000**, 346, 835-840.
42. Rueda, D., et al., *Mol Pharmacol*, **2000**, 58, 814-820.
43. Guzman, M., et al., *Biochem J*, **2000**, 347, 369-373.
44. Guzman, M., et al., *Mol Pharmacol*, **1998**, 54, 834-843.
45. Kolesnick, R., Kronke, M., *Annu Rev Physiol*, **1998**, 60, 643-665.
46. Sofia, R., et. al., *J Pharmacol Exp Ther*, **1978**, 186, 646-655
47. Buxbaum, D., *Psychopharmacology*, **1972**, 25, 275-280.
48. Guindon, J., and Beaulieu P., **2006**, 50, 814-823.
49. Guindon, J., et. al., *Pain*, **2006**, 121, 85-93.
50. Abrams, D., et. al., *Neurology*, **2007**, 68, 515-521.
51. Ellis, R., et. al., *Neuropsychopharmacology*, **2009**, 34, 672-680.
52. Svendsen, K., et al., *BMJ*, **2004**, 329, 253.
53. Zajicek, J., et. al., *Lancet*, **2003**, 362, 1517-1526
54. Rog, D., et. al., *Neurology*, **2005**, 65, 812-819
55. Amar, M., *Journal of Ethnopharmacology*, **2006**, 105, 1-25.
56. Hutcheon, A. W., et. al., *European Journal of Cancer and Clinical Oncology*, **1983**, 19, 1087-1090.
57. Compston, A., Coles, A., *Lancet*, **2008**, 372, 1502-17.
58. Tremlett, H., Oger, J., *J. Neurol.* **2004**, 251, 1297-303.
59. Croxford, J.L., Miller, S.D., *Drugs Today*, **2004**, 40, 663-676.
60. Guzman, M., et. al., *FEBS Lett*, **1998**, 436, 6-10

61. Sarker, K., et. al., *FEBS Lett*, **2000**, *472*, 39-44
62. Chan, G., et. al., *J. Neurosci*, **1998**, *18*, 5322-5332.
63. Chan, P. et. al., *Fundam Appl Toxicol*, **1996**, *30*, 109-117.
64. Di Marzo, V., et al., *Proc Natl Acad Sci USA*, **1998**, *95*, 8375-8380.
65. Di Marzo, V., et. al., *Endocrinology*, **2000**, *141*, 118-126.

Chapter Two

Synthetic Pathways towards Cannabinoid Analogues

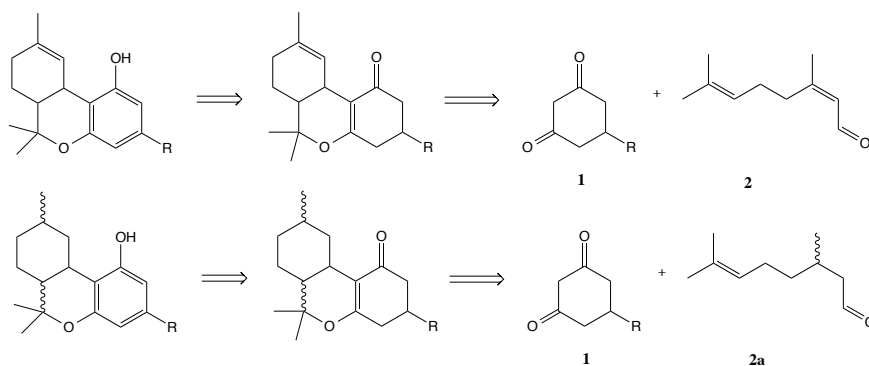
2.1 Introduction

With the increased interest in the great therapeutic potential of cannabinoids also comes the interest in finding more efficient methods for the facile synthesis of these compounds. Our synthetic pathways built off the seminal work of Teitze with the goal of providing pathways to both aromatic and non-aromatic cannabinoid analogues. These compounds were also computationally screened for their affinity for the CB₁ receptor (Chapter 3). In addition to this *in silico* screening, our cannabinoid analogues were biologically screened and preliminary studies showed they possessed therapeutic potential towards ALS.

2.2 Facile Synthesis of Cannabinoid Analogues

2.2.1 The Use of Non-olivetol Sources Towards Δ^1 -THC and Analogues

As seen in chapter one, the most notable approaches to Δ^1 -THC employ the use of olivetol to establish the 1,3-dioxo-5-alkylbenze counterpart moiety. One of our approaches to this synthesis, however, utilizes a non-aromatic precursor of olivetol (**1**) and initially citral (**2**) to first establish the three-ring conformation seen in the natural cannabinoids, followed by subsequent aromatization (Scheme 2.1). Citronellal (**2a**) (both racemic and enantiopure) was also employed to provide access to unnatural cannabinoid analogues.



Scheme 2.1. Retrosynthetic analysis utilizing a non-aromatic olivetol precursor.

The advantage to the synthetic pathway shown in scheme 2.1 is threefold: (1) Stereochemical control: The use of enantiopure citronellal also complete control over the stereochemical outcome of the non-aromatic cannabinoid (Figure 2.1a). (2) Both aromatic and non-aromatic cannabinoids can be obtained through regulation of the conjugation in the third ring of the cannabinoid skeleton (Figure 2.1b). (3) That same third ring can be functionalized with various functional groups or chains, or can even be truncated (Figure 2.1c).

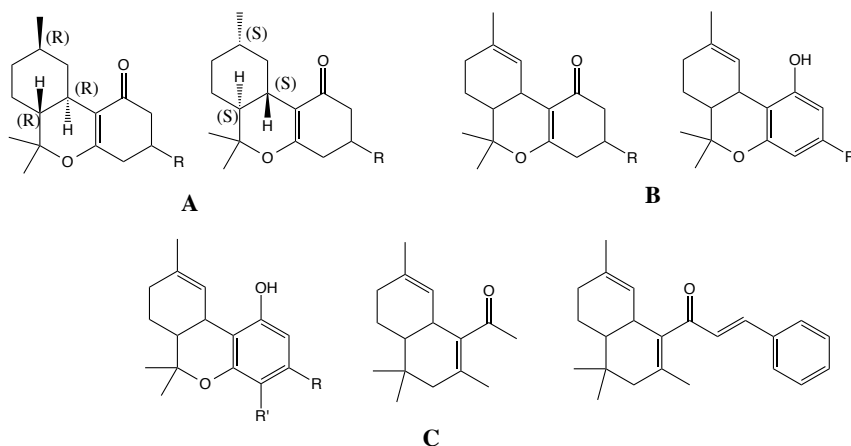
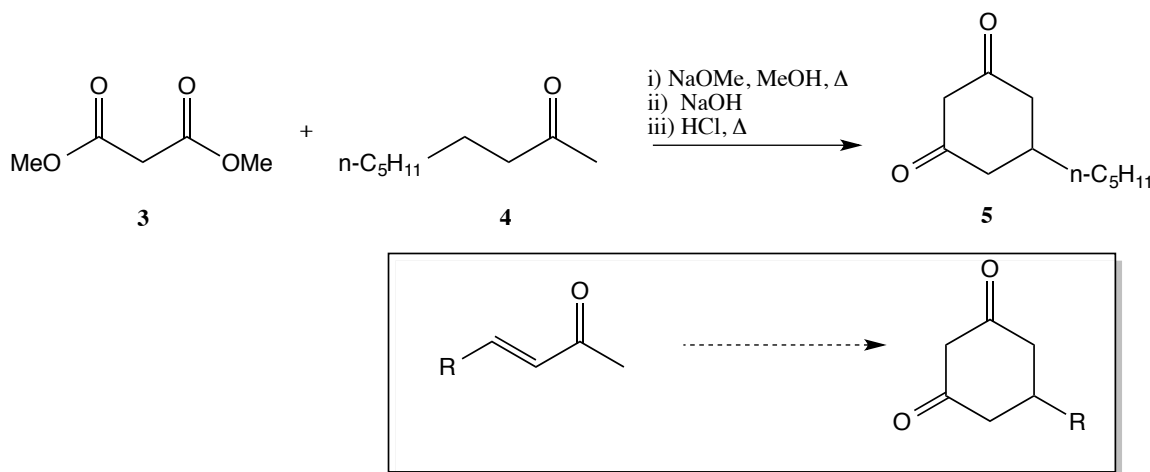


Figure 2.1. Advantages for utilizing non-olivetol sources in the synthesis of aromatic and non-aromatic cannabinoids.

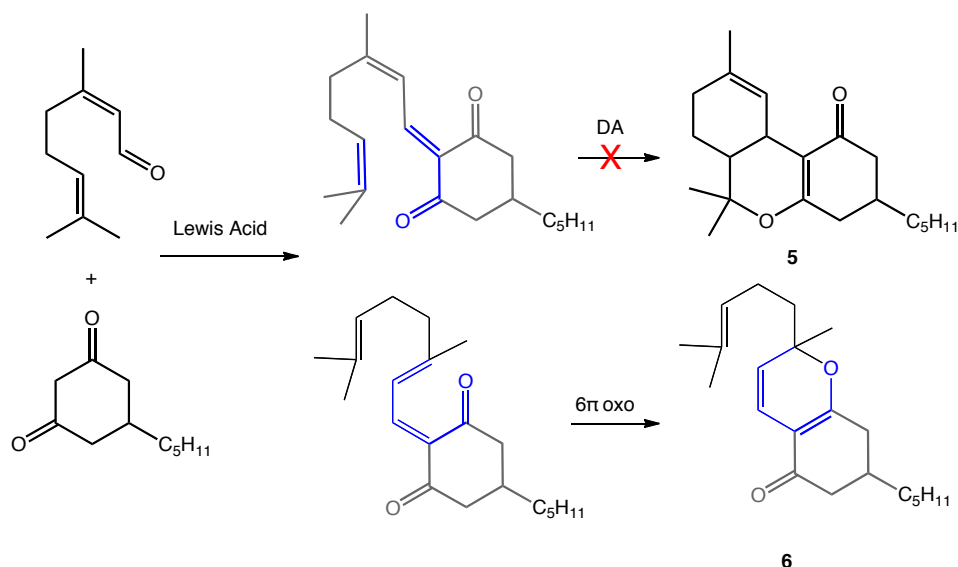
2.2.2 Synthesis of Perhydro- and Tetrahydro- Cannabinoid Analogues

The olivetol precursor was synthesized using dimethyl malonate **3** and 3-nonen-2-one **4** followed by saponification and decarboxylation to give 5-pentylcyclohexane-1,3-dione **5** in excellent yield (Scheme 2.2).¹ It should be noted that by varying the saturated carbon chain on the α,β -unsaturated methyl ketone, any desired side-chain could theoretically be incorporated into the non-aromatic precursor (see inset of Scheme 2.2).



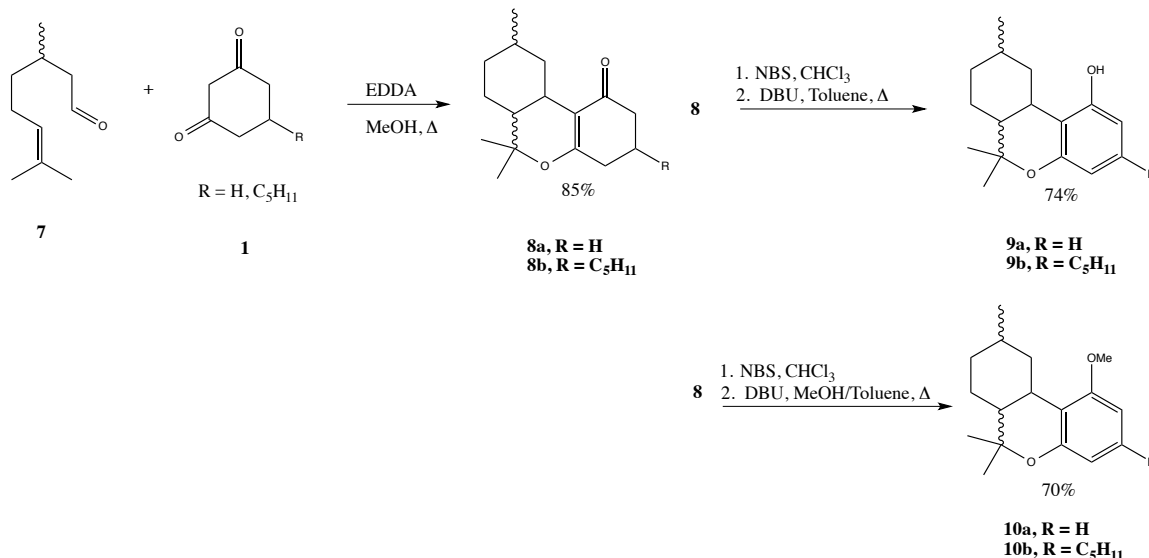
Scheme 2.2. Synthesis of non-aromatic olivetol precursor

With the olivetol precursor in hand, it was intended to perform a tandem Knoevenagel-Diels Alder reaction with citral to obtain **5** thereby building off of Tietze's work.² However, as seen in Scheme 2.3, the reaction followed an oxo- 6π electrocyclization to yield the perhydro analog of cannabichromene **6**.



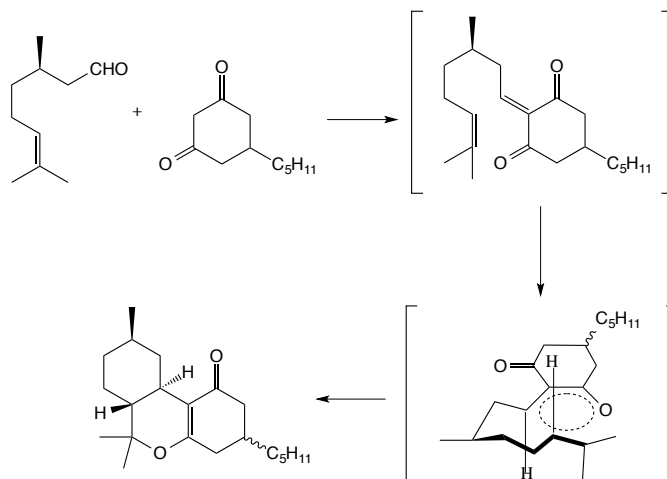
Scheme 2.3. Knoevenagel-oxo-6 π electrocyclization reaction of citral with olivetol precursor

A new pathway was then sought replacing citral with citronellal **7** with the intention of establishing the olefin functional group as the last step of the synthesis (Scheme 2.4). The reaction between citronellal and 5-pentylcyclohexane-1,3-dione was also well documented by Tietze² and was performed in the presence of ethylenediaminediacetate (EDDA), which is believed to catalyze the Knoevenagel and Diels Alder reaction.³ Initially, the following reactions were performed using 1,3-cyclohexanedione to confirm pathways as well as simplify NMR data. Racemic citronellal was condensed and subsequently cyclized onto **1** to give perhydrocannabinoid **8** in 85% yield. Aromatization was accomplished in two steps by bromination using NBS followed by elimination with 1,8-Diazabicycloundec-7-ene (DBU) in refluxing toluene (Scheme 2.4) to give analogue **9** which we've coined " Δ^0 -THC". It should also be noted that the anisole derivative **10** can be obtained by using a 50:50 mixture of methanol and toluene during the aromatization.



Scheme 2.4. Synthesis of “ Δ^0 -THC” **9** and its anisole derivative **10**.

Tietze also documented that by using enantiomerically pure citronellal, the stereochemistry of the 3,4 positions can be controlled (Scheme 2.5).² Calculations



Scheme 2.5. Transition state of stereochemically governed Diels Alder reaction

performed by our group (Semi-Emperical) verified this stereospecific control as well as indicating that the energy for the transition state to form a cis-3,4-cannabinoid is nearly

14 kJ/mol higher than its trans counterpart (Figure 2.2). This had a great potential for our synthesis as previous reports of stereochemical control required the use of chiral ligands and heavy metal catalysts (see chapter one), and this method could easily allow us to establish the trans-(3R, 4R) stereochemistry observed in natural Δ^1 -THC.

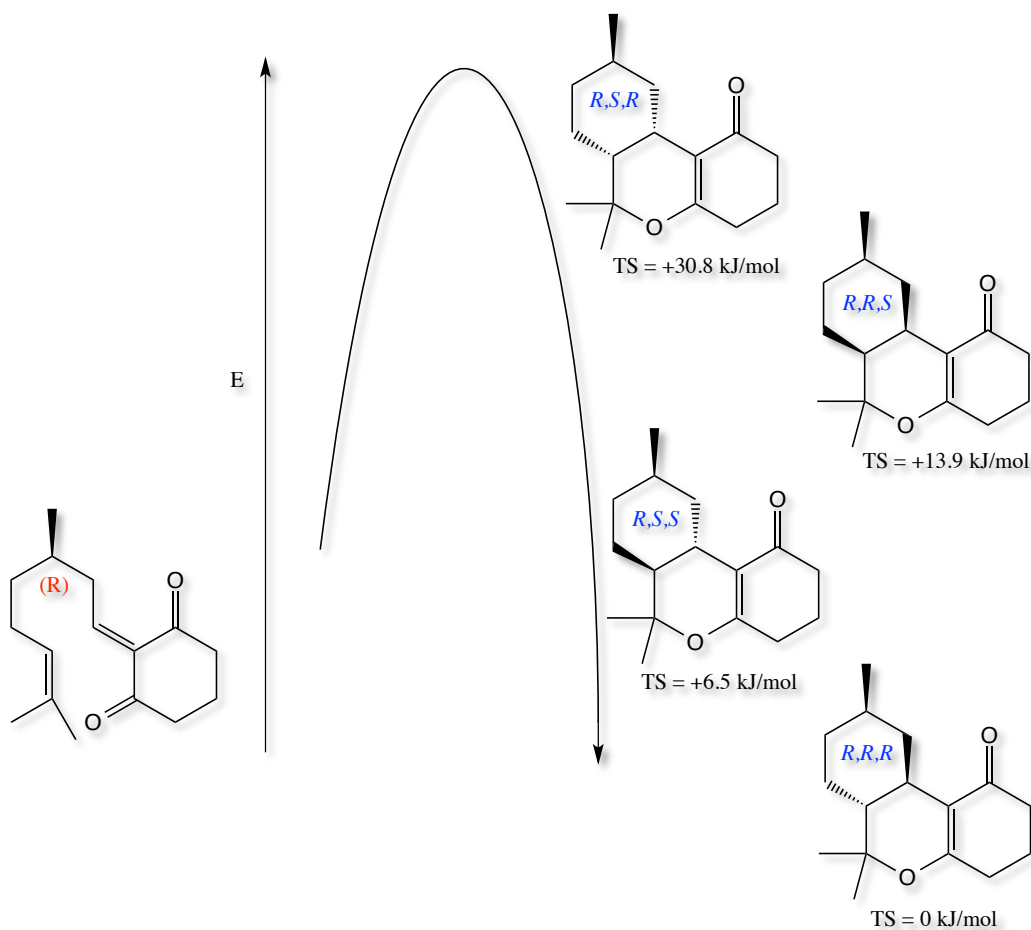


Figure 2.2. Computational results showing stereochemical control by enantiopure citronellal

Test reactions were then performed to determine the outcome of a free radical bromination with a subsequent E2 elimination in mind. Figure 2.3 depicts the possible centers for a free radical bromination. However, attempts to establish the desired

unsaturation through a free radical bromination followed by an E2 elimination were abandoned as the result in each case was the bromination of the phenolic ring. At this point we decided to revisit the possibility of utilizing citral.

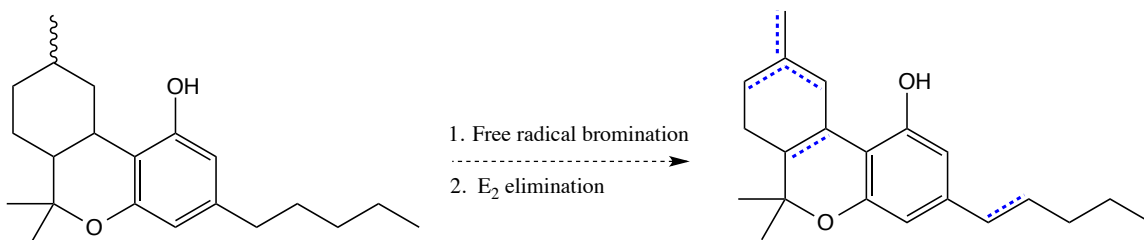
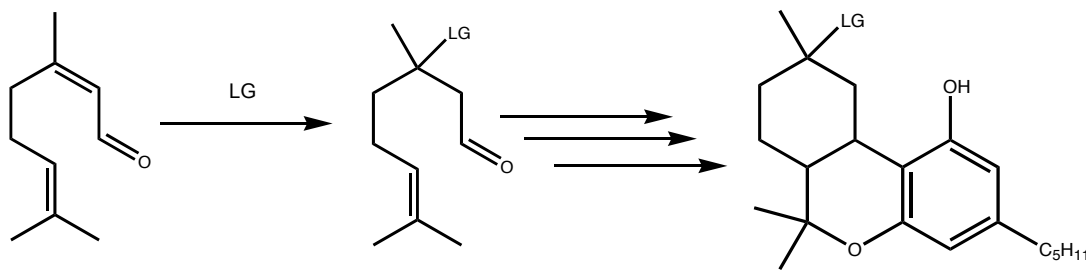


Figure 2.3. Possible outcomes (indicated in blue) for the free radical bromination of hexahydrocannabininol

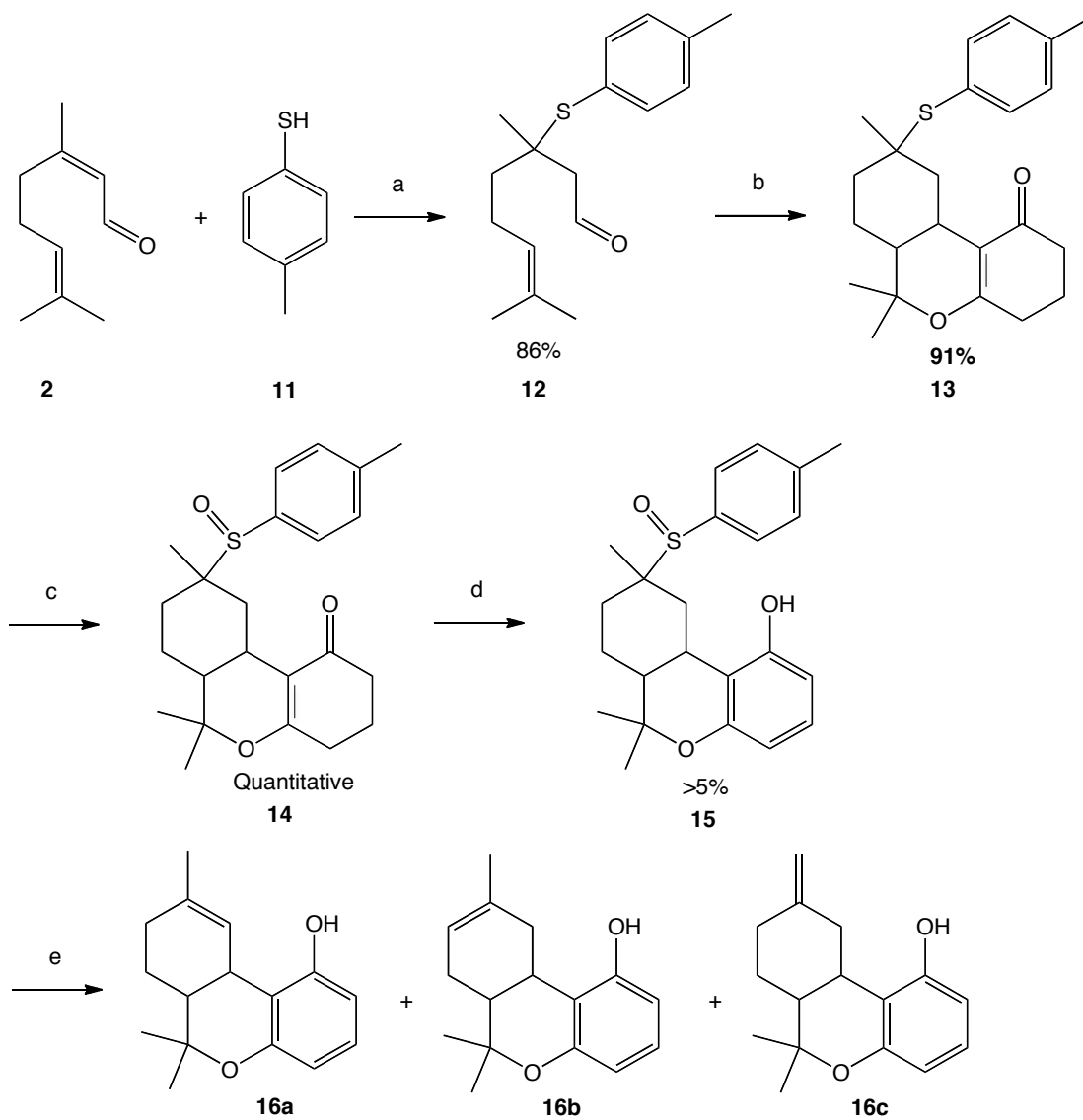
2.2.3 Revisiting Citral

The pathway utilizing citral and our olivetol precursor was re-examined with the goal to protect the α,β -unsaturation, perform the desired transformations, and remove the protecting group resulting in the reformation of the olefin (Scheme 2.6). We chose to use p-toluenethiol as the source of our protecting group as the Michael addition of thiols to citral is well documented,⁴ and the resulting thio ether, once oxidized to either a sulfoxide or sulfone, can be cleaved through various means to re-establish the olefin.



Scheme 2.6. Protection of citral

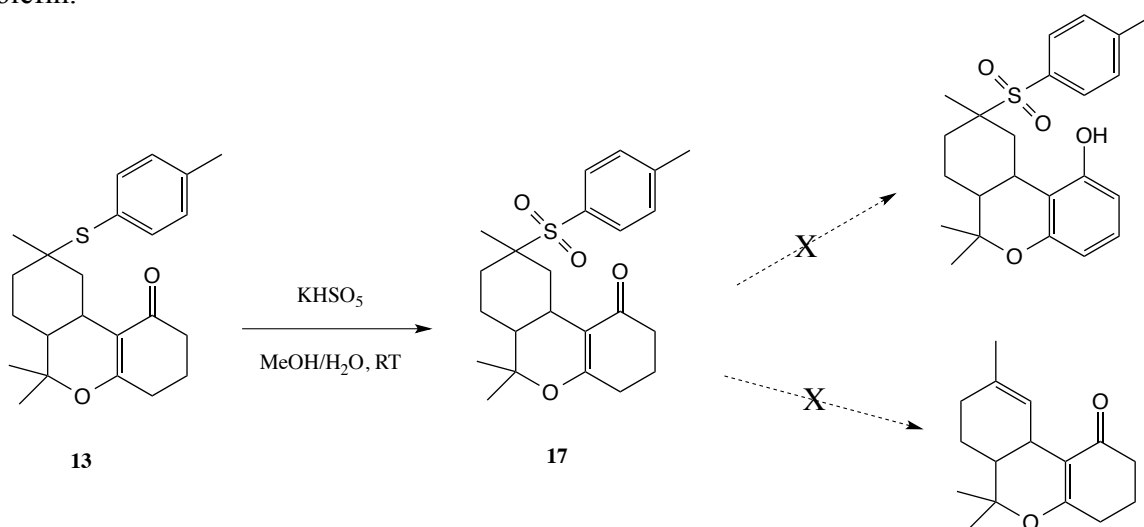
Citral **2** was added to p-toluenethiol **11** and the mixture was mounted on a solid support of KF/Alumina (approximately 50% KF by weight) to give thiocitronellal derivative **12** in 86% yield (Scheme 2.7). This reaction can either be accomplished in a microwave in about 30 minutes or by stirring in a sonicator for 4 hours. Perhydrocannabinoid **13** was obtained after an EDDA catalyzed tandem Knoevenagel/Diels-Alder reaction of **12** with readily available 1,3-cyclohexanedione. This dione was used in place of 5-pentylcyclohexane-1,3-dione for the purpose of testing the new synthetic pathway as well as simplifying interpretation of NMR data. It should be noted that addition of EDDA to a solution of the dione absent of aldehyde will lead to polymerization of the dione. Quantitative oxidation of thioether **13** to obtain sulfoxide **14** was accomplished using mCPBA. Attempts to oxidize **2** under the same conditions led to the epoxidation of the remaining double bond, therefore requiring the cyclization to **13** to occur before oxidation. Aromatization using NBS and DBU (as well as other methods) to obtain **15** proved difficult, as yields were often less than 5%. With the small amount obtained, **15** was mounted on silica and placed in a microwave at a temperature of 150°C. Preliminary NMR indicated the formation of three olefin peaks thought to represent the Δ^1 (**16a**), Δ^6 (**16b**), and exo (**16c**) olefinic hydrogens of their respective THC analogues. However, this could not be verified due to the small amount of starting material available as well as the harsh reaction conditions leading to decomposition. Continuing studies are underway to optimize the aromatization method to verify the results of the elimination of the sulfoxide.



a. KF/Alumina, sonication; b. 1,3-cyclohexanedione, EDDA, MeOH, Δ ; c. mCPBA, CHCl_3 , 0°C ; d. 1. NBS, CCl_4 , R.T. 2. DBU, Toluene, Δ ; e. silica, μwave , 200W, 150°C , 1 h.

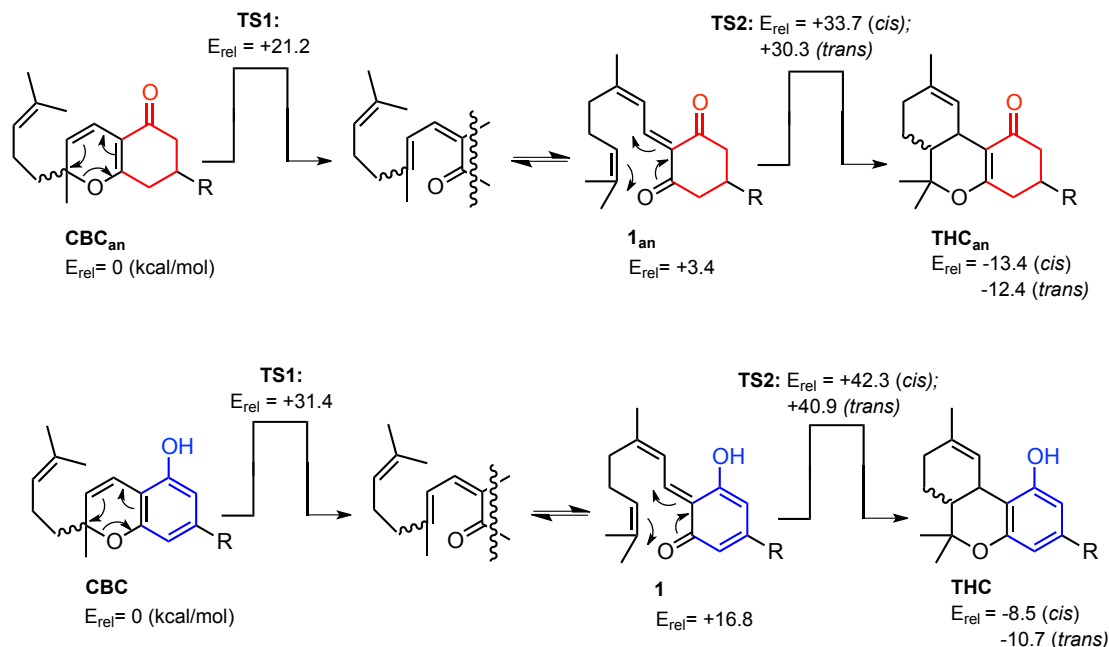
Scheme 2.7. Use of protected citral towards THC analogues

In order to lower the temperature conditions for the elimination of the thioether protecting group, thioether **13** was fully oxidized to sulfone **17** using Oxone[®] resulting in what should have been a more labile leaving group (Scheme 2.8). However, as before, attempts to aromatize **17** were met with poor yields. Also, attempts to eliminate the sulfone from **17** under various conditions did not lead to the reformation of the original olefin.



Scheme 2.8. Formation of sulfone **17**.

While other studies are underway to rectify the issues with aromatization and elimination of protecting groups, we turned our attention back to the work of Angie Garcia from our group who demonstrated the thermal isomerization of non-aromatic cannabichromene (CBC) analogues to non-aromatic THC analogues.⁵ Calculations performed by Garcia showed that the isomerization to non-aromatic THC is thermodynamically favored by 13.4 kcal for the cis isomer and 12.4 kcal for the trans isomer (Figure 2.4). In addition, the isomerization from aromatic CBC to Δ^1 -THC is thermodynamically favored by 8.5 kcal for the cis isomer and 10.7 kcal for the trans

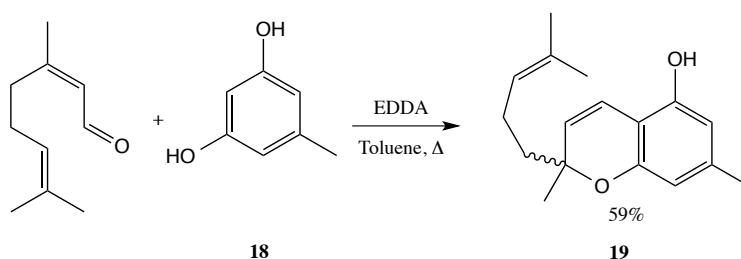


R = CH₃ (for simplifying DFT calculations)

Figure 2.4. Spartan calculations (B3LYP/6-31G*) performed by Angie Garcia for the starting materials, products, and transition states for the isomerization of non-aromatic and aromatic analogues of CBC

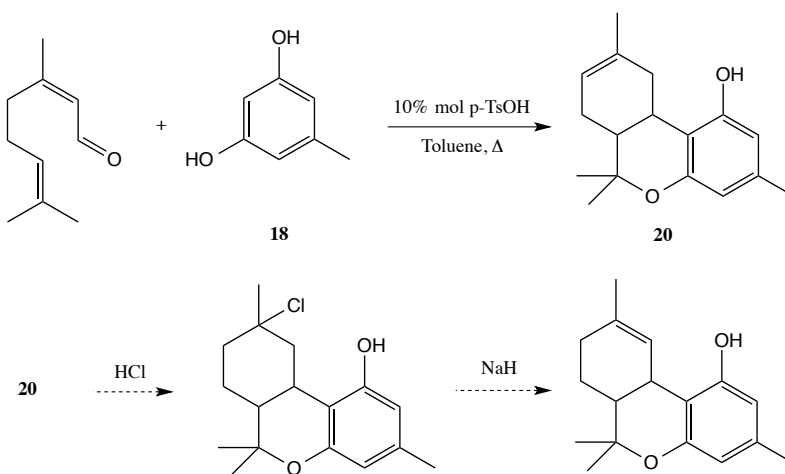
isomer. Therefore, if aromatic CBC could be obtained, the probability that it could isomerize to THC under certain conditions is theoretically possible.

In 2005, Yong Lee and Xue Wang reported the one step synthesis of CBC using citral and olivetol catalyzed by EDDA.⁶ This reaction can also be accomplished using primary amines such as t-butylamine or n-propylamine.⁷ Utilizing the EDDA catalyzed methodology, we condensed citral with orcinol (**18**) to give the methyl analog of CBC **19** in yields comparable to the original publication (Scheme 2.9). Attempts to isomerize **19** to the methyl Δ^1 -THC analog were unsuccessful as heating on silica led to decomposition of the starting material and reactions utilizing catalytic amounts of acid also led to a large amount of decomposition with trace amounts of unidentifiable cannabinoid products.



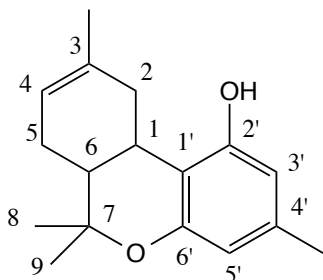
Scheme 2.9. Synthesis of CBC-Me.

However, a concurrent study of the reaction described in scheme 2.10 utilized a catalytic amount of *p*-toluenesulfonic acid instead of EDDA to give the methyl analog of Δ^6 -THC **20** in 15% yield. If desired, Δ^1 -THC could then be obtained by using the hydrochlorination/dehydrohalogenation methodology described by Mechoulam.⁸



Scheme 2.10. Synthesis of Δ^6 -THC-Me and potential isomerization to Δ^1 -THC-Me

Table 2.1 shows the comparison of the experimental ^{13}C -NMR data obtained for **20** compared to a literature reference set for Δ^6 -THC.⁹

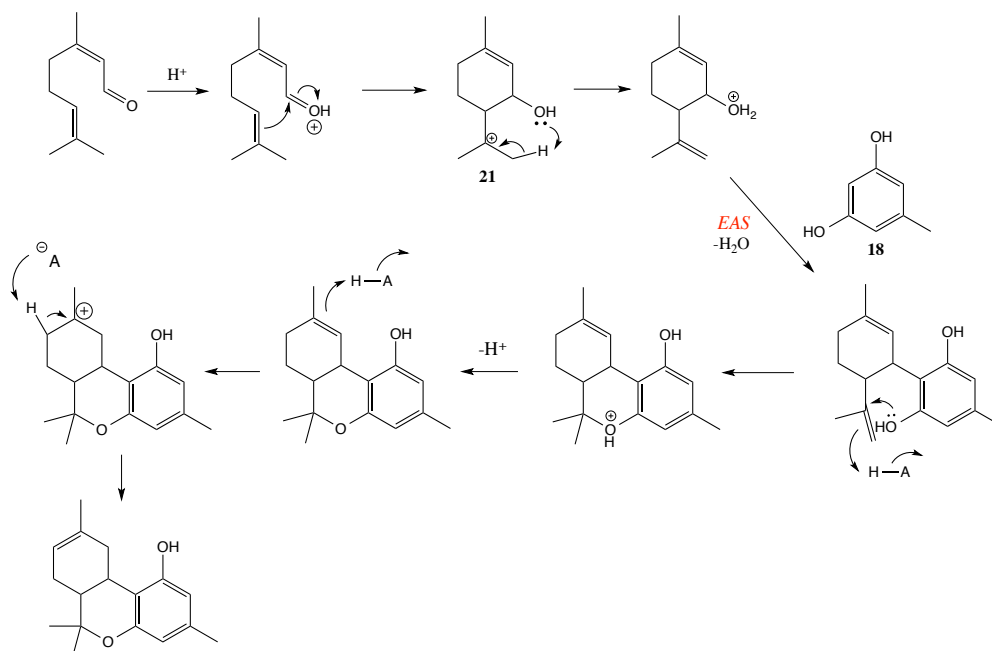


Position	Reference NMR	Experimental NMR
1	31.6	31.7
2	36.0	36.2
3	134.7	134.9
3-Me	23.5	23.7
4	119.3	119.5
5	27.9	27.8
6	44.8	45.0
7	76.7	77.4
8	27.6	27.7
9	18.5	18.7
1'	110.5	111.0
2'	154.8	155.0
3'	107.6	108.5
4'	142.7	138.0
5'	110.1	110.6
6'	154.8	155.1

Table 2.1. ^{13}C -NMR data for the comparison of experimental results to a reference set.

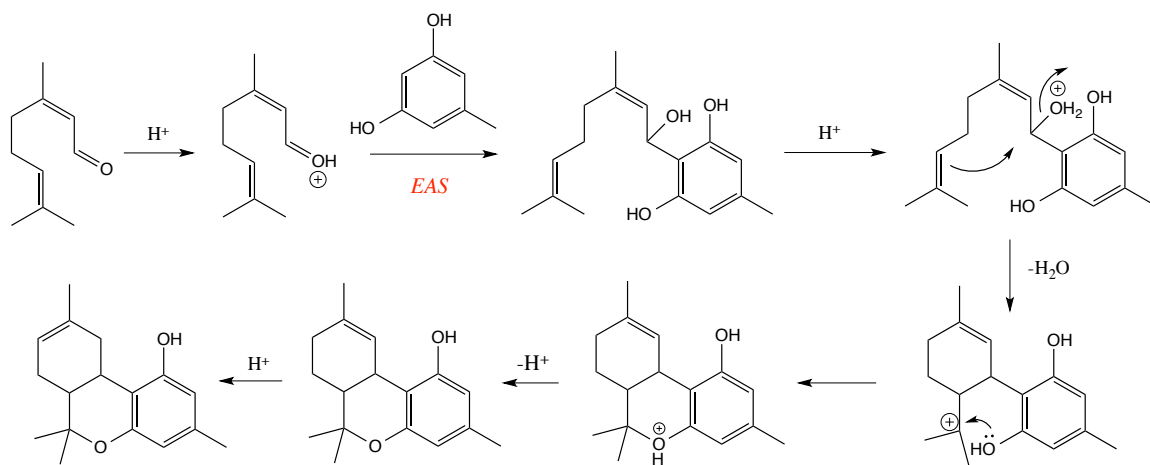
The formation of **20** could proceed through one of two possible mechanisms. Scheme 2.11 depicts a pathway where citral undergoes an acid catalyzed cyclization to form cation **21** followed by the electrophilic aromatic substitution onto **18**. The evidence for **21** was provided by Chrombie in 1975, where citral was mixed in a solution of TsOH

in dichloromethane absent olivetol.¹⁰ Initially, a Δ^1 -THC analog is formed, however, under most acidic conditions, high temperatures, and prolonged reaction times, Δ^1 -THC will isomerize to the more stable Δ^6 -THC isomer.¹¹



Scheme 2.11. Possible mechanistic pathway for the formation of the methyl analogue of Δ^6 -THC in which citral undergoes an acid catalyzed cyclization followed by an electrophilic aromatic substitution.

The second mechanistic pathway (Scheme 2.12) involves the electrophilic aromatic substitution occurring first followed by a cyclization to give a cannabinidiol cation. After the final cyclization and subsequent isomerization, the Δ^6 -THC analogue is obtained. Current studies are ongoing to determine the effect of solvent, temperature, and catalyst mole ratios on influencing the yield and distribution of THC isomers.



Scheme 2.12. Alternative mechanistic pathway for the formation of the methyl analogue of Δ^6 -THC in which the electrophilic aromatic substitution occurs first followed by cyclization.

2.3 The Pharmacological Potential of Δ^6 -THC

While a literature search for the pharmacotherapy of Δ^1 -THC will yield hundreds of results, it seems that the potential for Δ^6 -THC as a therapeutic agent has been somewhat overlooked. Mechoulam has demonstrated that Δ^6 -THC is in fact biologically active¹² and its psychotomimetic properties are much less notable than Δ^1 -THC.¹³ It should also be noted that Δ^6 -THC is much more stable than Δ^1 -THC to various chemical treatments including oxidation, and is much less expensive to synthesize than Δ^1 -THC.¹³ A 1994 study performed by Itzhak Wirgin and coworkers using rats induced with experiment autoimmune encephalomyelitis (EAE) demonstrated a significant reduction in the incidence and severity of neurological deficit upon treatment with Δ^6 -THC.¹⁴ In a

1995 study, Mechoulam administered Δ^6 -THC as an antiemetic to eight children (ages 3-13) undergoing antineoplastic treatments for various hematologic cancers.¹³ The results were the complete cessation of vomiting with negligible side effects (including the psychoactive effects normally associated with Δ^1 -THC).¹³ In 1999, an analog synthesized from Δ^6 -THC, 1',1'-dimethylheptyl-delta-6-tetrahydrocannabinol-11-oic acid (CT-3), was found to have analgesic and anti-inflammatory properties in rats.¹⁵ In 2010, Abdul-Kader Souid and coworkers demonstrated the toxicity of Δ^6 -THC towards Tu183, a highly malignant form of oral cancer, through the inhibition of the cellular respiration of Tu183 cells.¹⁶

One possible pharmaceutical target utilizing the previously presented synthetic methodology of Δ^6 -THC is an analogue to Sativex™. Currently prescribed to multiple sclerosis patients to alleviate neuropathic pain, spasticity, overactive bladder, and other symptoms, Sativex™ is a 1:1 mixture of (-)- Δ^1 -THC and cannabidiol (CBD) extracted from cannabis (Figure 2.5).¹⁷ The Δ^6 analogues of both of the components of Sativex™

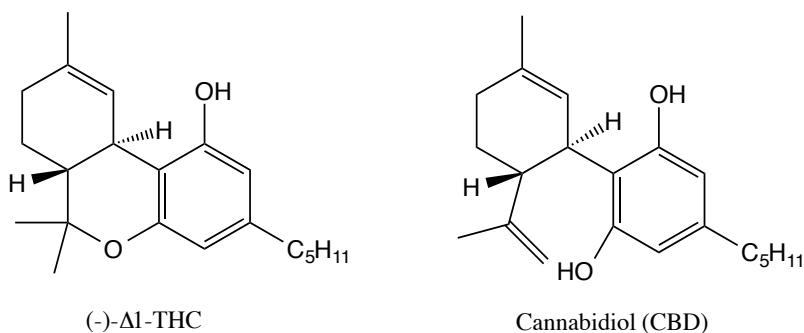
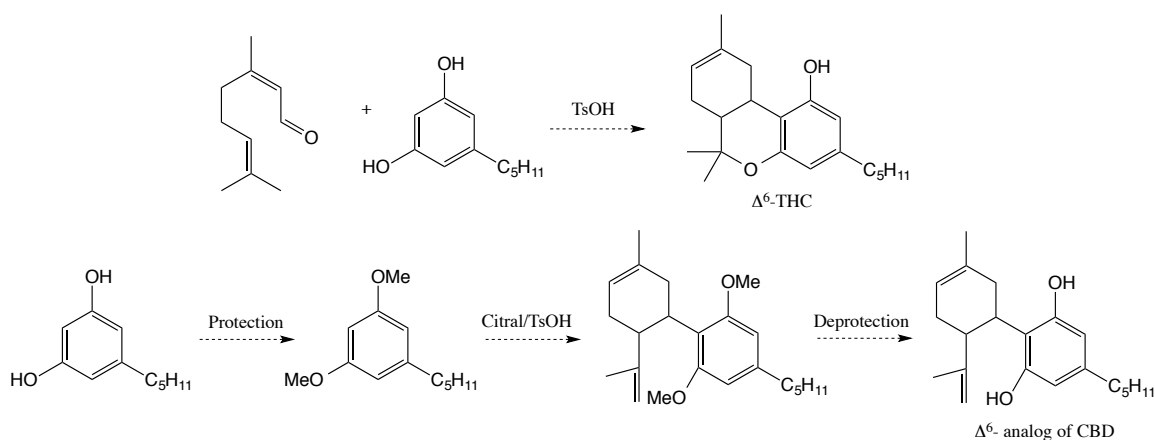


Figure 2.5. Structures of (-)- Δ^1 -THC and cannabidiol (CBD)

can theoretically be synthesized using the methods described in this chapter most likely at a lower cost compared to actually extracting the plant material (Scheme 2.13). In addition, psychotomimetic side effects could also be reduced as such properties for Δ^6 -THC are less than that of Δ^1 -THC.

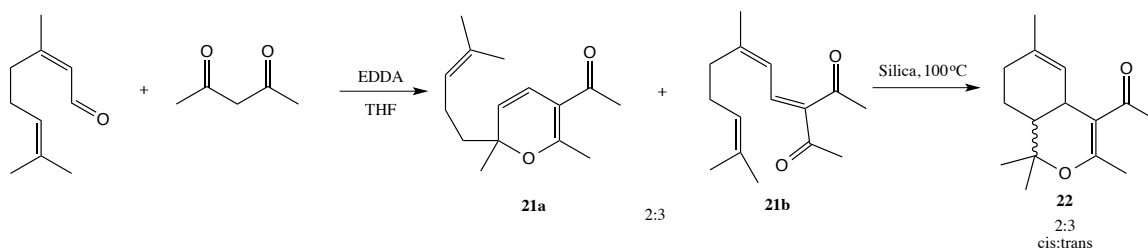


Scheme 2.13. Possible synthesis for a Δ^6 -analog of Sativex™

2.4 Synthesis of Other Cannabinoid Analogues

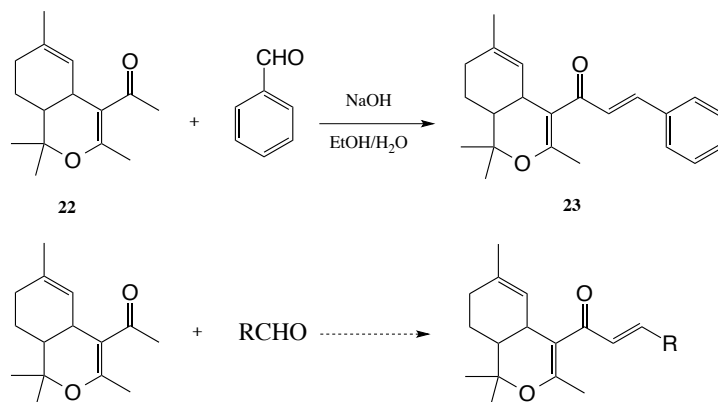
One of the goals in our group was to design and synthesize a small cannabinoid similar in structure to the natural cannabinoids yet still possibly retain the ability to bind well with the CB₁ receptor (see chapter 3 for the discussion on binding studies). Previous work had already demonstrated computationally that aromaticity is not a prerequisite for CB₁ receptor affinity.⁵ With that in mind, we set out to make a truncated cannabinoid analogue which completely eliminates the third ring of the typical cannabinoid skeleton. Our target, which we've designated "minimal" THC (**19**), is easily made in two steps from readily available starting materials.

Citral is condensed onto 2,4-pentanedione to afford a 2:3 mixture of pseudo-cannabichromene analog **21a** and **21b**. Longer reaction times do not increase the yield of **21b**. However, this was not detrimental to the overall synthesis as **21a** was still a viable starting material for the next step. Using methods developed in our lab to isomerize non-aromatic CBC analogues to non-aromatic THC analogues, the mixture of **21a** and **21b** was mounted onto silica and heated to 100°C to yield the cis/trans isomers of **22** in a ratio of 2:3 (Scheme 2.14). This is of interest because the ratio of products **21a** and **21b** led to the same ratio of cis/trans isomers of **22**. It is quite possible that uncyclized product **21a** is responsible for the formation of trans-**22**, and **21b** leads exclusively to cis-**22**. However, verification of this theory is still pending.



Scheme 2.14. Synthesis of “minimal” THC **19**.

Aldol condensations can also be utilized to functionalize the methyl ketone of **19**. Benzaldehyde was added to an ethanolic sodium hydroxide solution containing **19** to afford the α , β -unsaturated ketone **21** (Scheme 2.15). This methodology could possibly be expanded for a variety of aldehydes to further functionalize “minimal” THC and gain access to a large library of potential CB₁ ligands.



Scheme 2.15. The use of aldol condensations to functionalize “minimal” THC

2.5 Summary

While the effort to specifically synthesize Δ^1 -THC was met with numerous barriers, the investigation into utilizing a tandem Knoevenagel-Diels Alder and Knoevenagel-oxo- 6π -cyclization allowed us access to several cannabinoid analogues and the potential to produce libraries of cannabinoids from subsequent reactions such as aldol condensations. The one step synthesis of a Δ^6 -THC analogue provides a gateway into the exploration of Δ^6 -THC as a therapeutic agent comparable to Δ^1 -THC. In the next chapter, we will present *in silico* binding studies for some of the compounds from this chapter as well as other possible CB₁ ligands that can be synthesized using the methodologies shown. We will also present the biological screening of “minimal” THC as a potential therapeutic agent for ALS.

1. Focella, A., et. al., *J Org Chem*, **1977**, *42*, 3456-3457.
2. Tietze, L.F., *Chem Rev*, **1996**, *96*, 115-136.
3. Lee, Y., Hung, T., *Tetrahedron*, **2008**, *64*, 7338-7346
4. Lenardao, E., et. al., *Tet Lett*, **2007**, *48*, 6763-6766.
5. Marsella, M., Garcia, A., et. al., *J Amer Chem Soc*, **2009**, *131*, 16640-16641.
6. Lee, Y., Wang, X., *Bull. Korean Chem Soc*, **2005**, *26* 1933-1936.
7. Elsohly, M.; Turner, C.; *U.S. Patent No. 4,315,862*. Washington, DC: US.
8. Mechoulam, R.; Bruan, P.; Gaoni, Y., *J Amer Chem Soc*, **1967**, *89*, 4552-4554.
9. Verpoorte, R., et. al., *Phytochem. Anal.*, **2004**, *15*, 345-354.
10. Crombie, W.; Crombie, L., *Phytochemistry*, **1975**, 213-220.
11. Razdan, K., et. al., *J Org Chem*, **1981**, 949-953.
12. Mechoulam, R., *Marijuana; Chemistry, Pharmacology, Metabolism, and Clinical Effects*. Academic Press, New York, 1973.
13. Mechoulam, R.; Abrahamov, Aya; Abrahamov, Avraham; *Life Sciences*, **1995**, *56*, 2097-2102.
14. Wirguin, i., et. al., *Immunopharmacology*, **1994**, *28*, 209-214.
15. Dajani, E., et. al., *The Journal of Pharmacology and Experimental Therapeutics*, **1999**, *291*, 31-38.
16. Soud, A-K., et. al., *Pharmacology*, **2010**, *85*, 328-335.
17. GW Pharmaceuticals. <<http://www.gwpharm.com/SPC.aspx>>

Chapter Three

Computational and Biological Screening of Cannabinoid Analogues

3.1 Computational Binding Studies of Various Cannabinoids

Section 3.1.1 Introduction

Chapter one detailed some of the many therapeutic benefits of cannabinoids acting upon the CB¹ receptor. It would seem appropriate then to have a relatively simple and inexpensive methodology for screening synthetic cannabinoid targets *in silico* with the goal of identifying potential CB¹ ligands. Herein, we report the results of the *in silico* screening of some of the cannabinoids synthesized utilizing the methods presented in chapter two as well as compounds that could be made from the same methodologies. The results of preliminary biological studies demonstrating the therapeutic potential for some of our cannabinoid analogues towards the treatment of ALS will also be presented.

Section 3.1.2 Protocol for Obtaining Binding Data

Compounds to be screened for binding studies were built in MarvinSketch (part of the MarvinBeans® suite) and transferred as pdb files to PyRx.¹ Once the desired ligand(s) and receptor are selected, a box is generated to denote the binding site of the CB¹ receptor. A series of conformational poses are given as possible results, however, the accepted conformation must meet the following criteria: a docking score of -7.1 kcal/mol or lower (more negative), a hydrogen bond interaction with the Lys192 residue of CB1, and the side chain of the compound must be directed towards the Thr197, Tyr275, Trp279, and Met363 residues.⁸ This criteria is based on the standard result using

(-)- Δ^1 -THC as the native ligand (See Figure 3.1). (-)- Δ^1 -THC has a binding affinity of -7.1 kcal/mol.

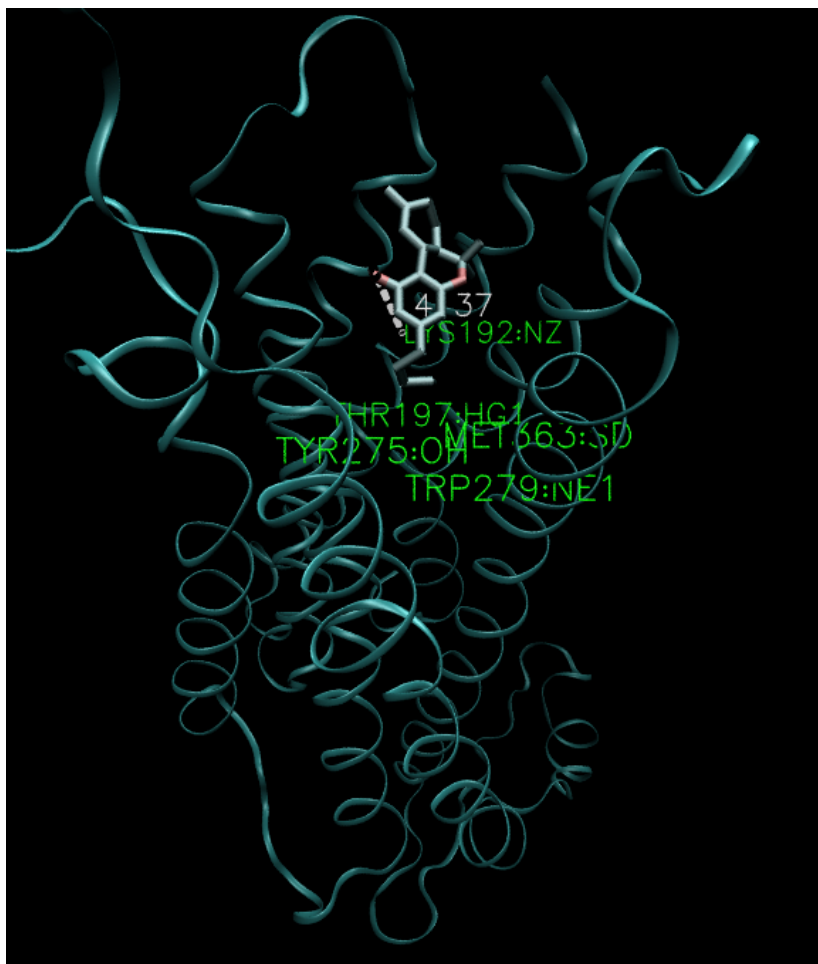


Figure 3.1. (-)- Δ^1 -THC docked into a modeled CB1 receptor. The receptor is represented by the green ribbon.

Section 3.1.3 Binding Studies of Known Cannabinoids Ligands

To serve as a control group, a variety of known cannabinoid ligands were screened to demonstrate their documented affinity towards the CB¹ receptor (Table 3.1). These compounds include phyto- and synthetic cannabinoids some of which are currently

used as a pharmaceutical treatment or involved in trials as a therapeutic agent. It was found that (-)- Δ^6 -THC has a slightly higher binding affinity than (-)- Δ^1 -THC for the CB¹

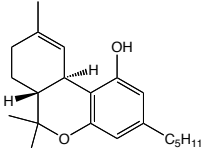
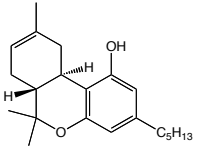
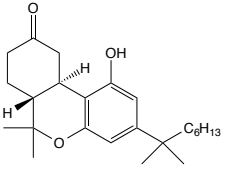
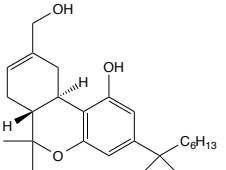
Ligand	H-Bond Distance with LYS192 (in Å)	Side Chain Interaction with Remaining Residues	Docking Score (in kcal/mol)
 (-)- Δ^1 -THC	4.37	Yes	-7.1
 (-)- Δ^6 -THC	3.34	Yes	-7.3
 R,R-Nabilone	4.42	Yes	-7.9
S,S-Nabilone	3.75	Yes	-6.9
 (-)-HU-210	3.57 (H-bonding is to the phenolic -OH)	Yes	-7.1

Table 3.1. Results of computational binding studies of phyto- and synthetic cannabinoids.

receptor as well a shorter H-bonding interaction. Since nabilone (CesametTM) is administered as a racemic mixture of the trans isomers, each isomer was analyzed separately both of which were found to have a good affinity towards CB¹. HU-210 is a synthetic cannabinoid found to be 100 to 800 times more potent than (-)- Δ^1 -THC and has

an extended duration of action.^{3,4} The (+) enantiomer was analyzed since it has been documented that (+)-HU-210 has almost all of the affinity for CB1 and the (-) enantiomer acts as an NMDA antagonist with neuroprotective effects.^{5,6} Since HU-210 has 2 hydroxyl groups that could potentially hydrogen bond with the LYS192 residue, the conformational pose that fulfilled all of our binding requirements was one in which the phenolic –OH interacted with the lysine residue.

Section 3.1.4 Binding Studies of Unnatural Stereoisomers of Δ^1 - and Δ^6 -THC

Table 3.2 presents the results of the computational binding studies of the unnatural (S,S-trans and cis-) stereoisomers of Δ^1 - and Δ^6 -THC. These isomers can be accessed through methods such as those presented in chapter one as well as those shown in the previous chapter. Cis- isomers of both Δ^1 - and Δ^6 -THC have binding affinities to CB¹ less than that of their natural counterparts and in addition, the cis isomers of Δ^6 -THC do not meet the criteria of having the alkyl side chain interacting with the four required residues described in section 3.1.2. However, the unnatural S,S-trans- isomers of both Δ^1 - and Δ^6 -THC have good affinities towards the CB¹ receptor in addition to meeting all the other criteria.

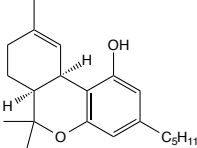
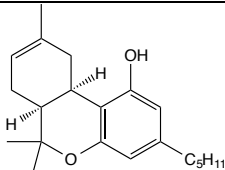
Ligand	H-Bond Distance with LYS192 (in Å)	Side Chain Interaction with Remaining Residues	Docking Score (in kcal/mol)
 3,4-(R,S)- Δ^1 -THC	5.17	Yes	-6.5
3,4-(S,R)- Δ^1 -THC	2.80	Yes	-6.2
3,4-(S,S)- Δ^1 -THC	4.66	Yes	-6.9
 3,4-(R,S)- Δ^6 -THC	3.13	No	-6.6
3,4-(S,R)- Δ^6 -THC	3.85	No	-6.2
3,4-(S,S)- Δ^6 -THC	5.19	Yes	-7.3

Table 3.2. Results of computational binding studies of the unnatural stereoisomers of Δ^1 - and Δ^6 -THC.

Section 3.1.5 Binding Studies of Methoxy Analogues of “ Δ^0 -THC”

Access to the methoxy derivatives of THC was presented in chapter 2 as well as the justification for the stereochemical induction into the trans- isomers of the analogues. Table 3.3 presents the results of the binding studies for the two enantiomers of the methoxy derivatives of “ Δ^0 -THC.” For these studies the interaction of the ligand with the LYS192 residue was defined as the attraction of the oxygen in the methoxy functional

group of the ligand to the N-H group of the lysine residue. Only the R,R,R-ligand has a binding affinity comparable to that of (-)- Δ^1 -THC.

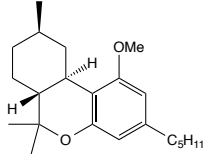
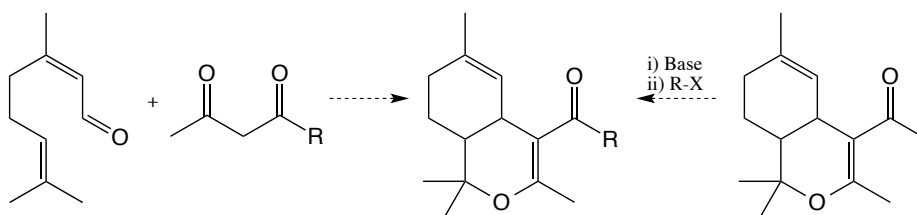
Ligand	H-Bond Distance with LYS192 (in Å)	Side Chain Interaction with Remaining Residues	Docking Score (in kcal/mol)
 1,3,4-(R,R,R)	5.44	Yes	-7.0
1,3,4-(S,S,S)	2.37	Yes	-6.5

Table 3.3. Results of computational binding studies of the trans isomers of the methoxy analogues of “ Δ^0 -THC.”

Section 3.1.6 Binding Studies of “Minimal” THC and Derivatives

Studies were done to determine the binding affinity of “minimal” THC (compound **24** from chapter 2) and derivatives either already synthesized (compound **25** from chapter 2) or those that could, in theory, be easily accessed. For example, derivatives with longer alkyl chains could be obtained either through varying the initial dione used or through the formation of an enolate followed by a substitution (Scheme 3.1).



Scheme 3.1. Possible pathways into “minimal” THC derivatives

Table 3.4 presents the results of the binding studies for “minimal THC,” compound **25**, and an alkyl substituted derivative that could be accessed as previously described. Since the original synthesis of “minimal THC” led to a mixture of cis/trans isomers, all four stereochemical isomers will be presented. For these studies the interaction of the ligand with the LYS192 residue was defined as the attraction of the carbonyl oxygen of the ligand to the N-H group of the lysine residue. The alkyl derivative tested includes an n-pentyl side chain.

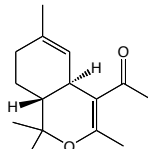
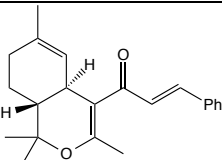
Ligand	H-Bond Distance with LYS192 (in Å)	Side Chain Interaction with Remaining Residues	Docking Score (in kcal/mol)
 3,4-(R,R)- 19	None	*Entire molecule interacts	-6.1
3,4-(S,S)- 19	None	*Entire molecule interacts	-6.4
3,4-(R,S)- 19	None	*Entire molecule interacts	-6.1
3,4-(S,R)- 19	None	*Entire molecule interacts	-6.0
 3,4-(R,R)- 25	3.10	Yes	-7.8
3,4-(S,S)- 25	2.98	Yes	-7.3
3,4-(R,S)- 25	5.40	No	-7.2
3,4-(S,R)- 25	3.18	Yes	-7.7

Table 3.4. Results of computational binding studies of “minimal” THC and derivatives.

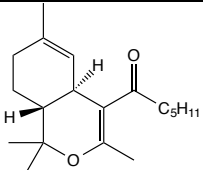
Ligand	H-Bond Distance with LYS192 (in Å)	Side Chain Interaction with Remaining Residues	Binding Affinity (in kcal/mol)
 3,4-(R,R)	3.27	No	-6.5
3,4-(S,S)	3.42	No	-6.6
3,4-(R,S)	2.92	Yes	-5.9
3,4-(S,R)	2.82	No	-6.1

Table 3.4. Continued

While the data suggests that all stereoisomers of **24** would bind poorly to CB¹ and none of them had an interaction with Lys192, all isomers had an interesting interaction with the remaining residues. Figure 3.2 shows how the isomers adopt almost the same

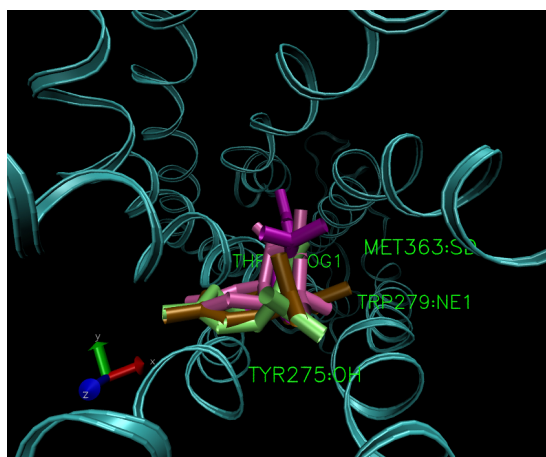


Figure 3.2. The interaction of the four stereoisomers of “minimal THC” with the Thr197, Tyr275, Trp279, and Met363 residues.

conformational pose in the same position within the Thr197, Tyr275, Trp279, and Met363 residues. The binding affinities for **25** suggest that this compound (with the exception of one stereoisomer) would have a higher affinity for CB¹ than (-)- Δ^1 -THC in contrast to the n-pentyl derivative which had poor binding affinities and most of the stereoisomers did not meet the requirement for the side chain to interact with the other four residues.

3.2 Biological Screening of “Minimal” THC

In collaboration with Dr. Milan Fiala at UCLA’s David Geffen School of Medicine, some of the cannabinoid analogues synthesized in our lab were tested as pharmaceutical targets for amyotrophic lateral sclerosis (ALS). ALS is a progressive neurodegenerative disease that affects nerve cells in the brain and the spinal cord having treatments designed to only slow the progression or manage the symptoms of the disease.⁷ A link has been demonstrated between ALS and the cannabinoids with THC showing some biological activity towards it.²

Our analogues were tested based on the inhibition of Interleukin-17, IL-17, in macrophages of ALS patients.⁹ Targeting the inhibition of IL-17 in ALS patients could lead to a potential ALS therapy since IL-17 is hypothesized to have a role in ALS.¹⁰

Figure 3.3 shows some of the results of this testing. Two of the analogues submitted for this testing were found to partially inhibit IL-17: a cannabichromene analogue made by Angie Garcia⁸ and compound **24**. The process involves using macrophages of ALS patients that are treated with stimulated superoxide dismutase

(SOD-1). Figure 3.3a is the negative control (not treated with SOD-1) and as such considered healthy (this is evidenced by the green color). Figure 3.3b represents macrophages treated with SOD-1 and is the positive control (represented by the red color). Figure 3.3c shows the results of the test of the cannabichromene analogue. The macrophage was treated with SOD-1 followed by the analogue. A partial inhibition of IL-17 is indicated by the primarily green color. Results for the testing of **24** led to the partial inhibition of IL-17 as well albeit to a smaller degree.¹¹

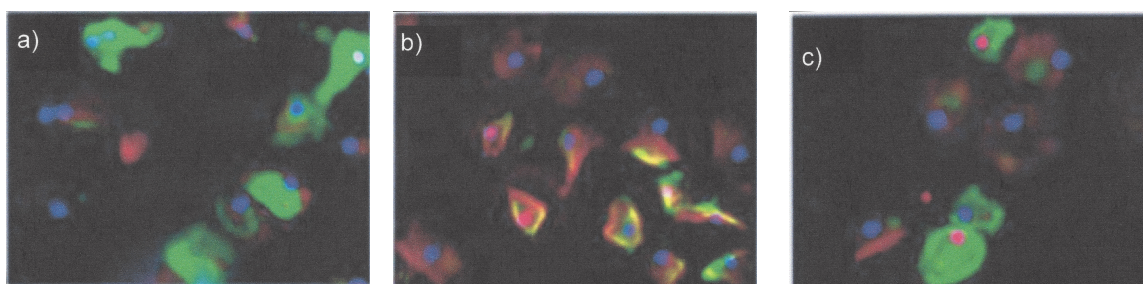


Figure 3.3. ALS macrophages treated with stimulated superoxide dismutase 1 (SOD-1). **a)** negative control (not treated with SOD-1); **b)** positive control (treated with SOD-1); **c)** treated with SOD-1 then cannabichromene analog.

A second study using our cannabinoid compounds was based on the inhibition of tumor necrosis factor alpha (TNF- α). As with IL-17, a high level of TNF- α is hypothesized to play a role in ALS.¹²⁻¹⁴ In preliminary studies, compound **24** was found to inhibit TNF- α at the nanomolar scale.¹¹

3.3 Summary

The data presented in this chapter has shown that cannabinoids synthesized using the methodologies described in chapter two can possibly act as CB¹ ligands. In addition, the conformational poses adopted by these compounds can give insights into building molecules that have structures unlike those of the classical cannabinoid. Biological screening of compound **24** demonstrated the partial inhibition of IL-17 as well as inhibition of tumor necrosis factor alpha and therefore could be useful in treating ALS.

1. PyRx: Trott, O.; Olson, A. J., *J. Comput. Chem.* **2010**, *31*, 455-461.
2. Picone, R.; et. al., *Mol. Pharmacol.*, **2005**, *68*, 1623-1635.
3. Mechoulam, R., et. al., *Experientia*, **1988**, *9*, 762–764.
4. Devane, W. A., et. al., *Journal of Medical Chemistry*, **1992**, *11*, 2065–2069.
5. Howlett, A.; Champion, T.; Wilken, G.; Mechoulam, R., *Neuropharmacology*, **1990**, *29*, 161.
6. Darlington, C, *IDrugs: The Investigational Drugs Journal*, **2003**, *6*, 976–979.
7. National Center for Biotechnology Information.
<<http://www.ncbi.nlm.nih.gov/pubmedhealth/PMH0001708/>>
8. Marsella, M., Garcia, A., et. al., *J Amer Chem Soc*, **2009**, *131*, 16640-16641.
9. Aggarwal, S.; Gurney, A., *J. Leukocyte Biol.*, **2002**, *71*, 1-8.
10. Fiala, M., et. al., *Journal of Neuroinflammation*, **2010**, *7*, 76.
11. Fiala, M.; Mizwicki, M.; Marsella, M., *Unpublished data*, **2009**.
12. Moreau, C., et. al., *Neurology*, **2005**, *65*, 1958-60.
13. Cereda, C., et. al., *J. Neuroimmunol.*, **2008**, *194*, 123-31.
14. Fujita, K.; Izumi, Y.; Kaji, R., *Brain and Nerve*, **2012**, *64*, 273-278.

Chapter Four

Simple Computational Methods of Predicting Asymmetric Reactions

4.1 Introduction

Since the pioneering work of Cram and co-workers in 1952¹, the prediction of the outcome of asymmetric induction has been the subject of intense study. The use of both steric and electronic arguments²⁻¹⁰ have met with generally good success to reckon asymmetric induction. While noncomputational models often require biased conformations and the more precise analysis of computational chemistry requires much time for high level theory calculations,^{5, 11-15} our work seeks to minimize the computational cost and yet maintain the integrity of accurate predictions for asymmetric induction.

4.2 Electrostatic Potential on LUMO surfaces (ESP@LUMO)

Previous work in our group performed by Nathan Wilmot utilized a quick computational method to project a visual interpretation of the frontier molecular orbital (FMO) onto a prochiral electrophile.¹⁶ This method does not require the user to infer steric arguments or calculate transition states, nor does it require biased conformations. While simplistic in nature this visualization method allowed for accurate prediction of stereochemical outcomes across a wide range of molecules. This approach integrates the following two concepts: (1) For any carbonyl functional group situated asymmetrically within, this asymmetry can be translated to electronic properties such as molecular orbital topology, electron density, and electrostatic potential which, in part, establishes the basis for prochiral facial selectivity by an attacking nucleophile.¹⁶ (2) FMO theory dictates that the most significant interaction between a nucleophile and an electrophile is that of the HOMO and LUMO. Therefore, the primary interest was the asymmetric topology of the

LUMO that exhibits an isosurface proximal to the reactive electrophilic site.¹⁶ To obtain these predictions the ESP of the reactive site was mapped onto the LUMO (Figure 4.1). The Gaussian 03 suite of software¹⁷ was used to first perform a PM3 geometry optimization on the global minimum conformer of the molecule of interest. This was followed by a HF/6-31G(d) single-point energy calculation using the structure from the previous step. The HF calculation allows one to generate an isosurface portraying the ESP

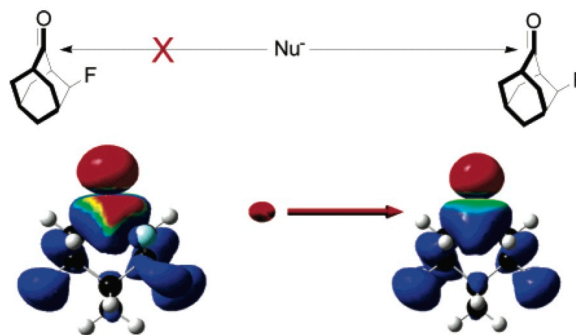


Figure 4.1. The ESP@LUMO map on fluoroadamantone

mapped onto the LUMO. The more electropositive face of the LUMO is determined through a visual inspection of this isosurface. A total of 19 examples of the reduction of a-chiral aldehydes and ketones were examined by Wilmot using the ESP@LUMO methodology which was able to correctly identify the major diastereomeric product with a predictive power of around 85%.¹⁶

4.3 The Use of ESP at a Reactive Site (ESP@RS) to Examine Both Steric and Electronic Effects

The previous computational method was further modified to emphasize the contribution of electrostatics to asymmetric induction rather than frontier molecular orbitals. While the ESP@LUMO method was highly accurate for most of the systems analyzed, some results demonstrated a gross asymmetry of the LUMO at the reactive carbon. In these cases the more electropositive face is not always the same distance from the reactive carbon and, therefore, may lead to erroneous predictions. To avoid this problem we chose to examine the sphere of electrostatic potential centered at the reactive site. This also allows us to examine sterics by viewing the ESP sphere on a Van der Waals (VDW) surface of the molecule. We have also expanded the methodology to include a wider array of reactions and have reinvestigated some results that do not match experimental results using the ESP@LUMO methodology.

Unlike the ESP@LUMO method, the computation of the ESP at the reactive site utilizes a single program (Spartan[®]), involves minimal steps, and avoids the time intensive *ab-initio* or DFT calculations. After the molecule of interest is built into the program, a MMFF equilibrium conformer is determined, and subsequent PM3 geometry optimization and electrostatic potential map are calculated. Final analysis requires mapping electrostatic potential onto a sphere that is centered on the reactive atom or functional group within the prochiral site of reactivity (“ESP @ RS,” whereby RS is the reactive site of the substrate). For such a surface, the alignment crosshairs (generated by the Spartan[®] program) are aligned perpendicular to the plane defined by the prochiral functional group, thus placing one crosshair on the *si*-face and one on the *re*-face. When

sterics is not a factor, facial selectivity is determined by the values of electrostatic potential at the intersection of each crosshair. The values may be either numerical or based on color-coding (blue being most positive and red being most negative ESP). Sterics will supercede electrostatics when significant encroachment at either crosshair by other functionality is seen, and determine the stereochemical outcome of the reaction. Significant encroachment is defined by having three of the four quadrants of the crosshair being blocked from attack. Figure 4.2 demonstrates the use of the ESP@RS method. The inset of Figure 4.2 shows the more reactive face of the same fluoroadamantone using the ESP@LUMO method. The asymmetry can be observed at the LUMO as sterics are de-emphasized.

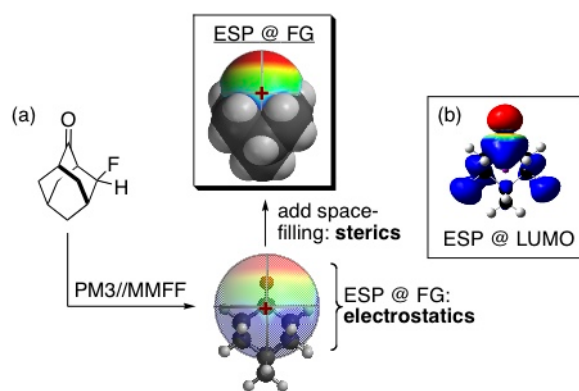


Figure 4.2. Comparison of ESP@RS method with ESP@LUMO method

4.4 Reduction of Asymmetric Carbonyls

The reduction of asymmetric carbonyls was originally examined using the ESP@LUMO method and revisited using the ESP@RS method. The predictive accuracy for this class of reaction was fairly high using the ESP@LUMO method, however, failed

for some reactions examining sterically hindered aldehydes. Since the ESP@RS method incorporates sterics into its protocol, the predictive power goes up without sacrificing any of the previously reported examples that were predicted correctly via LUMO@ESP.

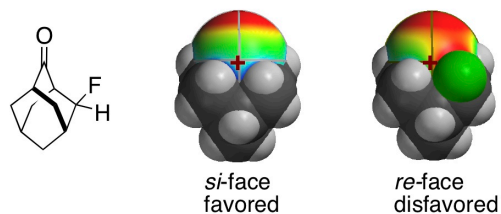


Figure 4.3. ESP@RS map on fluoradamantone

Figure 4.3 shows the *si* and *re* face of 3-fluoradamantone. The *si* face depicts a more electropositive (blue) result and the steric influence is slightly less than the *re* face. Experimentally, a nucleophile, specifically a hydride, attacks the *si* face with 100% selectivity. Further examples¹⁸⁻²² are shown in Table 4.1 and are reported as the electrostatic potential value and steric influence near the crosshair at each face as well as showing the ESP@RS maps.

Scheme	Major Isomer Face	Minor Isomer Face
<p>ca. 2:1</p>		
<p>67:33</p>		
<p>100:0</p>		
<p>de > 98%</p>		

Table 4.1. Results of predicting asymmetric reductions using ESP@RS methodology. ESP values are given at cross-hair points on each face of ketone carbon. ESP maps are shown for major and minor product faces in columns 2 and 3 respectively.

Scheme	Major Isomer Face	Minor Isomer Face
<p>Reaction scheme showing the reduction of a chiral ketone using Et_2BOMe and NaBH_4. The transition state is shown with energy values 10.17 and 21.72. The product is a diol with a de > 98%.</p>		
<p>Reaction scheme showing the allylic substitution of a chiral allylic chloride using Bu_2CuLi and ZnCl_2. The transition state is shown with energy values 3.99 and 0.601. The product is a 65:35 ratio of diastereomers.</p>		
<p>Reaction scheme showing the addition of CH_3Li to a chiral enone. The transition state is shown with energy values 4.55 and 2.10. The product is a 5:1 ratio of diastereomers.</p>		
<p>Reaction scheme showing the addition of CH_3MgBr to a chiral enone. The transition state is shown with energy values -0.34 and -1.11. The product is a 17.7:1 ratio of diastereomers.</p>		

Table 4.1. Continued

4.5 Silacyclopropanations

Using examples of stereoselective silacyclopropanation chemistry from the Woerpel group,^{24,25} we studied the silacyclopropanation reaction in terms of an electrophilic silicon attacking the more nucleophilic (more red) face of an asymmetric alkene. This is based on silicon having an NBO charge of 1^+ in the reactive $(\text{CH}_3)_2\text{Si}:$ species. Figure 4.4 illustrates an accurate prediction of this chemistry utilizing only ESP (4.4a) as well when sterics play a more evident role (4.4b).

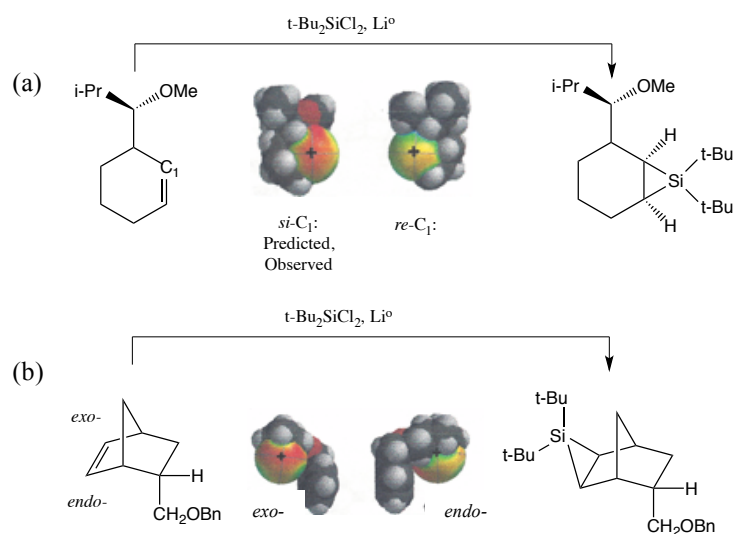


Figure 4.4. Prediction of silacyclopropanation reactions of chiral alkenes using ESP@RS methodology. The alkene has the role of the nucleophile and the more electronegative face (more red) should yield the major product.

While the preferred *exo*-face is more electronegative than the *endo*-face, sterics also demonstrates that the *endo*-face is blocked from electrophilic attack. A summary of our results is shown in Table 4.2.

Scheme	Major Isomer Face	Minor Isomer Face
<p>Reaction of a cyclohexene derivative with $t\text{-Bu}_2\text{SiCl}_2$ and Li^0. The alkene carbons have ESP values of -7.47 (red) and -2.06 (blue). The reaction yields two diastereomeric silacyclopropanes in a 96:4 ratio.</p>		
<p>Reaction of a cyclohexene derivative with $t\text{-Bu}_2\text{SiCl}_2$ and Li^0. The alkene carbons have ESP values of -6.39 (red) and -3.23 (blue). The reaction yields two diastereomeric silacyclopropanes in a 92:8 ratio.</p>		
<p>Reaction of a bicyclic alkene with $t\text{-Bu}_2\text{SiCl}_2$ and Li^0. The alkene carbons have ESP values of -7.95 (red) and 9.64 (blue). The reaction yields two diastereomeric silacyclopropanes in a 99:1 ratio.</p>		
<p>Reaction of a bicyclic alkene with $t\text{-Bu}_2\text{SiCl}_2$ and Li^0. The alkene carbons have ESP values of -7.01 (red) and 13.69 (blue). The reaction yields two diastereomeric silacyclopropanes in a 99:1 ratio.</p>		
<p>Reaction of a bicyclic alkene with $t\text{-Bu}_2\text{SiCl}_2$ and Li^0. The alkene carbons have ESP values of -1.78 (red) and 52.86 (blue). The reaction yields two diastereomeric silacyclopropanes in a 99:1 ratio.</p>		

Table 4.2. Summary of results in the prediction of silacyclopropanation reactions. ESP values are given at the center of the alkene for each face.

4.6 Aldol Reactions

This class of reactions was revisited from the LUMO@ESP method using the ESP@RS method resulting in an increase of 10% accuracy (from 80% to 90%). The use of a symmetrical sphere of electrostatic potential discounts the sometimes asymmetric LUMO. Also, including steric effects increases the predictive accuracy rather than looking only at the electronic properties.

For compounds that contain an open chain ether on the carbon beta to the aldehyde we have chosen to examine Li enolates as the reactive structures. Literature precedent has shown that these compounds form a chelate and therefore we have chosen to invoke this structure. Without the use of the Li enolate, the predictive power is very low (25% accuracy). However by using chelates the accuracy is nearly quantitative. Table 4.3 summarizes the results for predicting the reaction between chiral aldehydes and prochiral enolates using the ESP@RS method.²⁶⁻³⁵

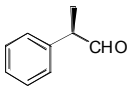
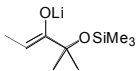
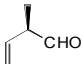
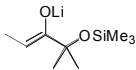
<u>Aldehyde</u>	<u>Enolate</u>	<u>(syn, syn):</u> <u>(syn, anti)</u>	<u>Re</u> <u>Face</u> <u>ESP</u>	<u>Si</u> <u>Face</u> <u>ESP</u>	<u>Re Face</u> <u>Sterics</u> <u>Effect</u>	<u>Si Face</u> <u>Steric</u> <u>Effect</u>	<u>Prediction</u> <u>(+, -)</u>
		81:19 (Felkin)	5.29	21.7	O	X	+
		75:25 (Felkin)	6.14	2.75	O	O	+

Table 4.3. Summary of ESP@RS prediction results for the aldol reaction. The face which has the more positive electrostatic potential value at the cross-hairs is that which should be favored electrostatically. Sterics implies that one face or the other of the aldehyde was blocked from participating in the aldol reaction. (+) indicates that the prediction was correct, while (-) indicates that the prediction did not match experimental results.

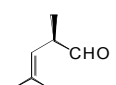
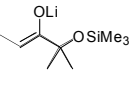
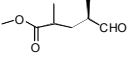
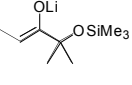
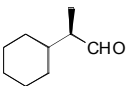
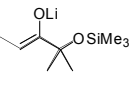
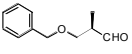
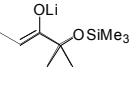
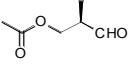
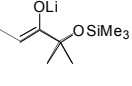
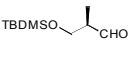
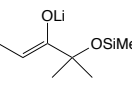
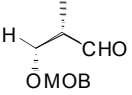
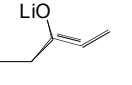
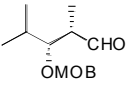
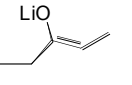
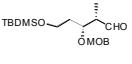
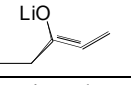
<u>Aldehyde</u>	<u>Enolate</u>	<u>(syn, syn):</u> <u>(syn, anti)</u>	<u>Re</u> <u>Face</u> <u>ESP</u>	<u>Si</u> <u>Face</u> <u>ESP</u>	<u>Re Face</u> <u>Sterics</u> <u>Effect</u>	<u>Si Face</u> <u>Steric</u> <u>Effect</u>	<u>Prediction</u> <u>(+, -)</u>
		94:6 (Felkin)	4.23	2.77	O	O	+
		45:55 (anti-Felkin)	64.5	9.63	X	O	+
		27:73 (anti-Felkin)	3.52	6.00	O	X	-
		33:67 (anti-Felkin)	-13.1	4.37	O	O	+
		23:77 (anti-Felkin)	-4.87	8.67	X	O	+
		21:79 (anti-Felkin)	1.71	3.96	O	O	+
		20:80 (anti-Felkin)	4.89	12.3	O	O	+
		87:13 (anti-Felkin)	100.4	2.98	X	O	-
		93:7 (anti-Felkin)	2.51	-25.9	O	Partial-X	+

Table 4.3. Continued

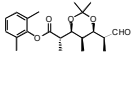
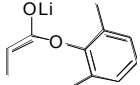
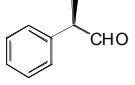
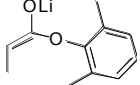
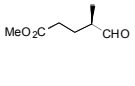
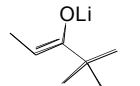
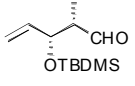
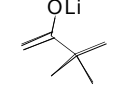
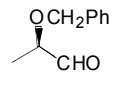
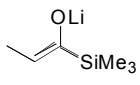
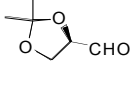
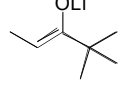
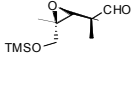
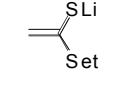
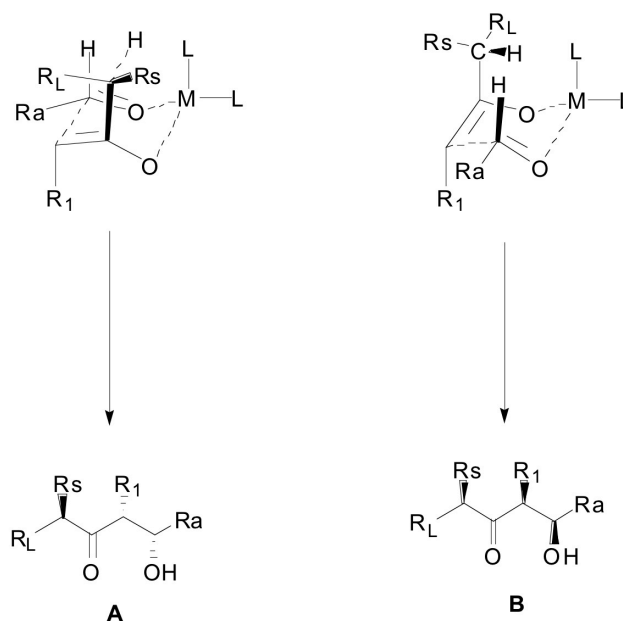
<u>Aldehyde</u>	<u>Enolate</u>	<u>(syn, syn):</u> <u>(syn, anti)</u>	<u>Re</u> <u>Face</u> <u>ESP</u>	<u>Si</u> <u>Face</u> <u>ESP</u>	<u>Re Face</u> <u>Sterics</u> <u>Effect</u>	<u>Si Face</u> <u>Steric</u> <u>Effect</u>	<u>Prediction</u> <u>(+, -)</u>
		2,3-anti- 3,4-syn <i>Anti-Felkin</i>	9.46	5.67	O	O	-
		2,3-anti- 3,4-syn 80:20 (Felkin)	5.29	21.73	O	X	+
		syn, syn (74:26) Felkin	5.72	1.69	O	O	+
		3,4-anti (88:12) <i>anti-Felkin</i>	2.51	12.94	O	X	+
		2,3-syn, 3,4-anti (79:17) <i>Anti-Felkin</i>	4.29	-3.37	Partial-X	O	+
		2,3-syn, 3,4-anti (85:15) <i>Anti-Felkin</i>	16.2	2.85	Partial-X	O	+
		syn (10:1) Felkin	5.50	5.75	O	O	+

Table 4.3.

4.7 Reactions of Chiral Enolates with Prochiral Aldehydes

Ten chiral *Z*-enolates and their reactions with prochiral aldehydes were analyzed. The success rate for this class of reaction is 90%. Scheme 4.1 depicts the two possible transition state templates and resulting products. This is due to the fact that the enolates are *Z*-enolates and the ESP of the aldehyde is essentially symmetric. Both *syn* products

are possible and the enantioselectivity is determined by the facial selectivity of the enolate.



Scheme 4.1. Possible transition state conformations and products in the Aldol reaction between a prochiral aldehyde and chiral enolate.

The PM3 methodology had to be adjusted for the amide enolates to account for systematic errors in this computational method. The ESP@RS method for amides therefore is as follows: MMFF conformer search followed directly by HF/3-21G* single point energy calculation on the lowest energy conformation and ESP determined by this step. Table 4.4 shows the results using this series of enolates.³⁶ While the local structure of the enolates is relatively the same, there are fairly dramatic differences in the remaining structure of these enolates. In almost each case severe sterics is rarely evident and our ESP@RS method can readily predict the stereochemical outcome of all reactions

based solely on electrostatic properties. While the relative enantioselectivity can differ largely between different aldehydes with reactions of a common enolate, the major product is always consistent, which further validates our method (see Table 4.4).

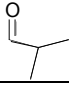
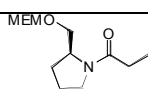
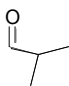
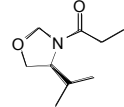
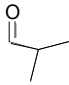
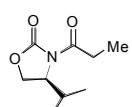
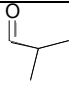
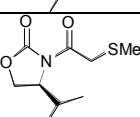
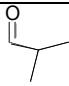
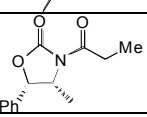
Aldehyde	Enolate	(syn, anti): (syn, syn)	<i>Re</i> Face ESP	<i>Si</i> Face ESP	<i>Re</i> Face Steric Effect	<i>Si</i> Face Steric Effect	Prediction (+, -)
		2:96	-26.72	-16.27	O	O	+
		98.3:0.5	-17.28	-21.72	O	O	+
		99.8:0.2	-11.97	-12.90	O	O	+
		98.4:1.6	-14.94	-15.15	O	O	+
		0.2:99.8	-15.35	-9.43	O	O	+

Table 4.4. Summary of results in predicting the aldol reaction between 2-methylpropanal and chiral enolates containing amides. The predicted attacking face is that which has the more electronegative value.

We also studied enolates that contain silyl ether functionality at the carbon alpha to the carbonyl carbon.³⁷⁻⁴⁰ The ESP@RS methodology resulted in a 80% success rate for these substrates (see Table 4.5). There was very little steric influence on either face of the reactive carbon, and all reactions can be predicted using purely electronic arguments. It is unclear why the one example (Entry 4) does not give an accurate result given the

similarities to Entry 5.

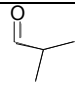
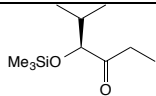
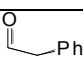
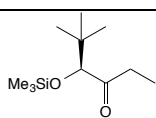
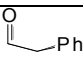
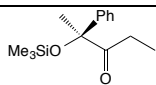
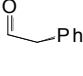
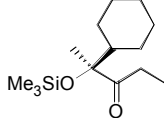
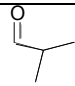
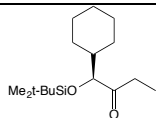
<u>Aldehyde</u>	<u>Enolate</u>	<u>(syn, anti):</u> <u>(syn, syn)</u>	<u>Re Face</u> <u>ESP</u>	<u>Si Face</u> <u>ESP</u>	<u>Re Face</u> <u>Steric</u> <u>Effect</u>	<u>Si Face</u> <u>Steric</u> <u>Effect</u>	<u>Prediction</u> <u>(+, -)</u>
		26:74	-14.05	-10.12	O	O	+
		13:87	-10.74	-6.26	X	O	+
		14:86	-20.54	-13.28	O	O	+
		6:94	-4.27	-10.96	O	O	-
		>99:1	-10.45	-16.09	O	O	+

Table 4.5. Summary of results in predicting the aldol reaction between prochiral aldehydes and chiral enolates. The predicted attacking face is that which has the more electronegative value.

4.8 Summary

Both the ESP@LUMO and ESP@RS methodologies are useful computational tools in that they utilize the *global minimum* conformations of substrates and are therefore inexpensive molecular mechanics conformation searches. Also, this global minima gives a common starting point for all substrates and reactions studied, thereby eliminating any uncertainty as to what the reactive conformation may be for a particular substrate. The ESP@RS method did demonstrate to be a better predictive method especially in difficult cases such as the Aldol reaction where the Felkin-Anh

methodology has shown to perform rather poorly. In addition, the ESP@RS allows the application of an accurate VDW surface onto a substrate and therefore, sterics and electrostatics can be inspected simultaneously.

1. Cram, D. J.; Elhafez, F. A. A., *J Amer Chem Soc*, **1952**, *74*, 5828-5835
2. Anh, N. T.; Eisenstein, O., *Tetrahedron Lett.*, **1976**, *3*, 155-158
3. Burgi, H. B.; Dunitz, J. D.; Lehn, J. M.; Wipff, G., *Tetrahedron*, **1974**, *30*, 1561-1572.
4. Burgi, H. B.; Dunitz, J. D.; Shefter, E., *J Amer Chem Soc*, **1973**, *93*, 5065-5067.
5. Anh, N. T.; Eisenstein, O.; Lefour, J.-M.; Dau, M.-E, *J Amer Chem Soc*, **1973**, *95*, 6146-6147
6. Karabostos, G. J., *Tetrahedron Lett.*, **1972**, *52*, 5289-5292.
7. Karabostos, G. J., *Tetrahedron Lett.*, **1967**, *49*, 4911-4914.
8. Karabostos, G. J., *J Amer Chem Soc*, **1967**, *89*, 1367-1371.
9. Conforth, J. W.; Cornforth, M. R. H.; Methew, K. K., *J Chem Soc*, **1959**, 112-127.
10. Cherest, M.; Felkin, H.; Prudent, N., *Tetrahedron Lett.*, **1968**, *18*, 2199-2204.
11. Wu, Y. D.; Houk, K. N., *J Amer Chem Soc*, **1987**, *109*, 908-910.
12. Cee, V. J.; Cramer, C. J.; Evans, D. A., *J Amer Chem Soc*, **2006**, *128*, 2920-2930.
13. Chao, I.; Shih, J. H.; Wu, H. J., *J Org Chem*, **2000**, *65*, 7523-7533.
14. Paddon-Row, M.N.; Wu, Y.-D.; Houk, K. N., *J Amer Chem Soc*, **1992**, *114*, 10638-10639.
15. Wu, Y. D.; Li, Y.; Na, J.; Houk, K. N., *J Org Chem*, **1993**, *58*, 4625-4628.
16. Wilmot N., Marsella, M., *Org Lett*, **2006**, *8*, 3109-3112.
17. Gaussian 03, Revision B.3, Frisch, M. J.; Trucks, G. W.; Schlegel, H. B.; Scuseria, G. E.; Robb, M. A.; Cheeseman, J. R.; Montgomery, Jr., J. A.; Vreven, T.; Kudin, K. N.; Burant, J. C.; Millam, J. M.; Iyengar, S. S.; Tomasi, J.; Barone, V.; Mennucci, B.; Cossi, M.; Scalmani, G.; Rega, N.; Petersson, G. A.; Nakatsuji, H.; Hada, M.; Ehara, M.; Toyota, K.; Fukuda, R.; Hasegawa, J.; Ishida, M.; Nakajima, T.; Honda, Y.; Kitao, O.; Nakai, H.; Klene, M.; Li, X.; Knox, J. E.; Hratchian, H. P.; Cross, J. B.; Bakken, V.; Adamo, C.; Jaramillo, J.; Gomperts, R.; Stratmann, R. E.; Yazyev, O.; Austin, A. J.; Cammi, R.; Pomelli, C.; Ochterski, J. W.; Ayala, P. Y.; Morokuma, K.; Voth, G. A.; Salvador, P.;

- Dannenberg, J. J.; Zakrzewski, V. G.; Dapprich, S.; Daniels, A. D.; Strain, M. C.; Farkas, O.; Malick, D. K.; Rabuck, A. D.; Raghavachari, K.; Foresman, J. B.; Ortiz, J. V.; Cui, Q.; Baboul, A. G.; Clifford, S.; Cioslowski, J.; Stefanov, B. B.; Liu, G.; Liashenko, A.; Piskorz, P.; Komaromi, I.; Martin, R. L.; Fox, D. J.; Keith, T.; Al-Laham, M. A.; Peng, C. Y.; Nanayakkara, A.; Challacombe, M.; Gill, P. M. W.; Johnson, B.; Chen, W.; Wong, M. W.; Gonzalez, C.; and Pople, J. A.; Gaussian, Inc., Wallingford CT, 2004.
18. Mengel, A.; Reiser, O., *Chem Rev*, **1996**, *99*, 1191-1223.
 19. Kaselj, M.; leNoble, W.J., *J Org Chem*, **1996**, *61*, 4157-4160.
 20. Wipf, P.; Kim, Y. T., *J Amer Chem Soc*, **1994**, *116*, 11678-11688.
 21. Danishefsky, S., et al., *Tetrahedron*, **1986**, *42*, 2809-2819.
 22. Solladie, G., et al., *J Org Chem*, **1995**, *60*, 7774-7777.
 23. Lee, W. D.; et. al., *Tetrahedron*, **2004**, *60*, 6657-6664.
 24. Driver, T.G., Woerpel, K.A., *J Amer Chem Soc*, **2003**, *125*, 10659-10663.
 25. Driver, T.G., Franz, A. K., Woerpel, K.A., *J Amer Chem Soc*, **2002**, *124*, 6524-6525.
 26. Tschamber, T., Waespesarcevic, N., Tamm, C., *Helv. Chem. Acta*, **1986**, *69*, 621-625.
 27. Heathcock, C. H., In *Asymmetric Synthesis*, Morrison, J. D., Ed. Academic Press: New York, 1984; Vol. 3, P 111.
 28. Young, S. D. Ph.D. Thesis, University of California, Berkeley, 1982.
 29. Masamune, S., Ellingboe, J.W., Choy, W., *J Amer Chem Soc*, **1982**, *104*, 5526-5528
 30. Heathcock, C. H., Pirrung, M. C., Montgomery, S. H., Lampe, J., *Tetrahedron*, **1981**, *37*, 4087-4095.
 31. Heathcock, C. H., Buse, C. T., Kleschick, W. A., Pirrung, M. C., Sohn, J. E., Lampe, J., *J Org Chem*, **1980**, *45*, 1066-1081.
 32. Patel, D., et. al., *J Amer Chem Soc*, Driver, T.G., Woerpel, K.A., *J Amer Chem Soc*, **2003**, *125*, 10659-10666.

33. Evans, D., et. al., *Tetrahedron Lett.*, **1990**, *31*, 6129-6132.
34. Myers, A. I., Hudspeth, J. P., *Tetrahedron Lett.*, **1981**, *22*, 3925-3928.
35. Heathcock, C. H., et. al., *J. Org. Chem.*, **1980**, *45*, 3846-3856.
36. Evans, D., Takacs, J. J., *Tetrahedron Lett.*, **1980**, *21*, 4233-4236.
37. Heathcock, C. H., et. al., *J. Org. Chem*, **1981**, *46*, 2290-2300.
38. Heathcock, C., H., et. al., *J Amer Chem Soc*, **1979**, *101*, 7077-7079.
39. Masamune, S., et. al., *Angew Chem Int Ed*, **1980**, *19*, 557-558.
40. Masamune, S., et. al., *J Amer Chem Soc*, **1981**, *103*, 1566-1568.

Appendix A

Experimental Procedures and Spectroscopic Data

Compound 1

Dimethyl malonate (6.650 g, 50.3 mmol) and sodium methoxide (2.400g, 44.6 mmol) were dissolved in dry MeOH in a 3 neck round bottom flask. 3-nonen-2-one (5.000 g, 35.7 mmol) was added in portions and the mixture was refluxed for 3 hours. After cooling to RT, the solvent was removed *in vacuo*, and the resulting oil was then dissolved in 30 mL of DI H₂O and washed 3 times with 5 mL of CHCl₃. The aqueous layer was acidified using conc. HCl and the mixture was allowed to stand overnight. The crystals were filtered from the mixture and transferred to another 3 neck round bottom flask. 200 mL of 2 M KOH solution was added to the flask and the solution was refluxed for 2 hours. Concentrated HCl (approximately 40 mL) was then added slowly and portion-wise and refluxed at 115°C until an oil bubbler indicated that the evolution of CO₂ gas had ceased. The reaction was washed twice with dilute acid followed by two portions of DI H₂O. The crude product was recrystallized from hexane (5.86 g, 90% yield). Physical properties and spectra data were identical to those stated in literature.

Compounds 8a and 8b

Cyclohexanedione **1** (R = H, 4.00 g, 25.9 mmol) was dissolved in 22 mL of MeOH in a 3 neck round bottom flask equipped with a stir bar. Citronellal (3.195 g, 28.5 mmol) was added followed by EDDA (1.167 g, 6.475 mmol) and the reaction was heated at 60°C for

5 hours. Hexane was added and the reaction was washed twice with dilute acid and twice with DI H₂O. After drying with MgSO₄ and filtering the crude mixture, the solvent was evaporated *in vacuo*. The product was purified by column chromatography over silica gel eluting with hexane/ethyl acetate (10:1) yielding **8a** (5.47 g, 85% yield). **8b** is obtained using **1** (R = C₅H₁₁) with comparable yields. Physical properties and spectra data for both **8a** and **8b** were identical to those stated in literature.

Compounds **9a** and **9b**

8a (1.32 g, 5.31 mmol) was dissolved in 10 mL of CCl₄ in a 3 neck round bottom flask equipped with a stir bar. N-bromosuccinamide (945 mg, 5.31 mmol) was then added and the reaction was stirred under nitrogen at room temperature for 24 hours. The solids were filtered off, and the solvent removed *in vacuo*. The residue was dissolved in 8.5 mL of toluene and 1.24 mL (8.30 mmol) of 1,8-diazabicyclo[5.4.0]undec-7-ene (DBU) was added. The reaction was then refluxed for 2 hours and quenched with dilute aqueous acid. The organic layer was washed once with dilute base and twice with DI H₂O. After drying with MgSO₄ and filtering the crude mixture, the solvent was evaporated *in vacuo*. The product was purified by column chromatography over silica gel eluting with hexane/ethyl acetate (7:1) yielding **9a** (968 mg, 74% yield). **9b** is obtained in the same manner with comparable yields. Physical properties and spectra data for both **9a** and **9b** were identical to those stated in literature.

Compounds **10a** and **10b**

8a (3.64 g, 14.7 mmol) was dissolved in 37 mL of CCl₄ in a 3 neck round bottom flask equipped with a stir bar. N-bromosuccinamide (2.61 g, 14.7 mmol) was then added and the reaction was stirred under nitrogen at room temperature for 24 hours. The solids were filtered off, and the solvent removed *in vacuo*. The residue was dissolved in 30 mL of a 1:1 mixture of toluene/MeOH and 4.40 mL (29.4 mmol) of DBU was added. The reaction was then refluxed for 2 hours and quenched with dilute aqueous acid. The organic layer was washed once with dilute base and twice with DI H₂O. After drying with MgSO₄ and filtering the crude mixture, the solvent was evaporated *in vacuo*. The product was purified by column chromatography over silica gel eluting with hexane/ethyl acetate (7:1) yielding **10a** (2.68 g, 70% yield). **10b** is obtained in the same manner with comparable yields. Physical properties and spectra data for **10b** were identical to those stated in literature. The spectra data for **10a** is as follows: ¹H-NMR (300 MHz, CDCl₃) δ 7.05 ppm (td, 1H), 6.48-6.45 (dd, 1H), 6.43-6.41 (dd, 1H), 3.82 (s, 3H), 3.05-3.01 (m, 1H), 2.53-2.43 (td, 1H), 1.89-1.85 (m, 2H), 1.67-1.62 (m, 1H), 1.48-1.45 (m, 2H) 1.40 (s, 3H), 1.24 (t, 1H), 1.08 (s, 3H), 0.97 (d, 2H), 0.80-0.65 (q, 1H). ¹³C-NMR (400 MHz, CDCl₃) δ 159.35, 155.07, 127.31, 110.84, 103.55, 102.63, 63.72, 55.35, 49.51, 35.85, 33.15, 28.37, 27.94, 22.89, 19.06, 15.15. *Data is for a mixture of diastereomers. Isolation of stereoisomers proved to be difficult. Due to peak overlap, multiplicity and integration cannot be accurately determined for individual isomers. HRMS (m/z): [M+]⁺ calcd for C₁₇H₂₄O₂, 260.1776; found 260.1768.

Compound 12

Method A. Citral (2.00 g, 13.1 mmol) and p-toluenethiol (1.63 g, 13.1 mmol) were added to a single neck round bottom flask. KF/Alumina (0.816 g, 50% by mass of p-toluenethiol) was added and the flask was placed in a microwave (300 W) under vacuum for 10 min. The product was filtered off the KF/Alumina by washing with ethyl acetate. The solvent was evaporated *in vacuo* and the residue purified by column chromatography over silica gel eluting with hexane/ethyl acetate (20:1) yielding **12** (3.27 g, 91%).

Method B. The aforementioned mixture was agitated constantly in a sonicator for 5 hours. The product was filtered as mentioned before and purified in the same manner. Yields obtained from this method are comparable to those from Method A. ¹H-NMR (300 MHz, CDCl₃) δ 9.95 (t, 1H), 7.38 (d, 2H), 7.12 (d, 2H), 5.07 (t, 1H), 2.45 (d, 2H), 2.37 (s, 3H), 2.20-2.17 (m, 2H), 1.69 (s, 3H), 1.64 (s, 3H), 1.60 (t, 2H), 1.36 (s, 3H). ¹³C-NMR (400 MHz, CDCl₃) δ 202.31, 139.66, 137.72, 132.40, 129.87, 127.35, 123.61, 52.55, 49.76, 46.01, 26.37, 25.88, 23.20, 21.43, 17.93.

Compound 13

1,3-cyclohexanedione (1.55 g, 13.8 mmol) was dissolved in 12 mL of MeOH in a 3 neck round bottom flask equipped with a stir bar. **12** (3.00 g, 13.8 mmol) was added followed by EDDA (0.497 g, 2.76 mmol) and the reaction was heated at 60°C for 5 hours. Hexane was added and the reaction was washed twice with dilute acid and twice with DI H₂O. After drying with MgSO₄ and filtering the crude mixture, the solvent was evaporated *in vacuo*. The product was purified by column chromatography over silica gel eluting with

hexane/ethyl acetate (7:1) yielding **13** (4.65 g, 91% yield). $^1\text{H-NMR}$ (300 MHz, CDCl_3) δ 7.57 (d, $J = 8.04$ Hz, 2H), 7.15 (d, $J = 7.87$ Hz, 2H), 2.94 (m, 2H), 2.39 (t, 1H), 2.32 (s, 3H), 2.30-2.21 (m, 2H), 1.87-1.85 (m, 2H), 1.78 (m, 1H) 1.64-1.61 (m, 1H), 1.57 (m, 2H), 1.49-1.45 (m, 2H), 1.33 (s, 3H), 1.27-1.19 (m, 2H), 1.15 (s, 3H), 1.08 (s, 3H), 0.81 (m, 1H). $^{13}\text{C-NMR}$ (400 MHz, CDCl_3) δ 197.55, 170.80, 138.82, 138.12, 129.41, 128.54, 114.40, 80.31, 50.50, 49.29, 41.14, 39.65, 37.77, 31.76, 29.85, 29.62, 27.43, 23.96, 21.45, 20.50, 19.89. *Data is for a mixture of diastereomers. Due to peak overlap, multiplicity and integration cannot be accurately determined for individual isomers. HRMS (m/z): $[\text{M}]^+$ calcd for $\text{C}_{23}\text{H}_{30}\text{O}_2\text{S}$, 370.1967; found 370.2064.

Compound 14

13 (415 mg, 1.12 mmol) was dissolved in CHCl_3 in a round bottom flask equipped with a stir bar. The flask was placed in an ice bath for 15 minutes before *m*-chloroperoxybenzoic acid (284 mg, 1.40 mmol) was added over a period of 5 minutes. The reaction was stirred at 0°C for 2 hours before quenching with a solution of concentrated KHCO_3 . The organic layer was washed once with dilute acid and twice with DI H_2O . After drying with MgSO_4 and filtering the crude mixture, the solvent was evaporated *in vacuo* yielding **14** (422 mg, 98%). NMR revealed the transformation to the desired product to be complete and therefore purification was not necessary. $^1\text{H-NMR}$ (300 MHz, CDCl_3) δ 7.99 (d, $J = 8.26$ Hz, 2H), 7.38 (d, $J = 8.05$ Hz, 2H), 3.22-3.15 (m, 2H), 2.86 (dd, 1H), 2.40 (s, 3H), 2.32-2.21 (m, 4H), 1.92-1.85 (m, 2H), 1.80-1.74 (m, 1H), 1.65-1.21 (m, 1H), 1.42-1.37 (m, 2H), 1.33 (s, 3H), 1.25-1.21 (m, 2H), 1.11 (s, 3H),

1.04 (s, 3H), 0.81 (m, 1H). ^{13}C -NMR (400 MHz, CDCl_3) δ 197.88, 171.28, 144.67, 132.97, 131.13, 129.41, 114.14, 80.58, 61.72, 48.47, 37.67, 37.28, 32.73, 29.77, 28.81, 22.77, 27.40, 24.31, 21.82, 20.43, 19.88. *Data is for a mixture of diastereomers. Due to peak overlap, multiplicity and integration cannot be accurately determined for individual isomers. HRMS (m/z): $[\text{M}]^+$ calcd for $\text{C}_{23}\text{H}_{30}\text{O}_3\text{S}$, 386.1916; found 386.1904.

Compound 17

In a 3-necked, round-bottom flask equipped with a stirbar was added 252 mg of oxone (0.410 mmol) and 2 mL of DI H_2O . This mixture was cooled in an ice bath for 15 minutes. Afterwards, a solution of 76 mg (0.205 mmol) of **13** in 2 mL of MeOH was added dropwise over 5 minutes. The reaction was then stirred at room temperature for 4 hours. The MeOH is removed *in vacuo*, and the remaining solution extracted three times with CH_2Cl_2 . The organic layer was dried with MgSO_4 , filtered and the solvent removed *in vacuo*. The white solid obtained was recrystallized from hexane to yield 71 mg of **17** (87% yield). ^1H -NMR (300 MHz, CDCl_3) δ 7.69 (d, 2H), 7.35, (d, 2H), 3.10 (m, 1H), 2.73-2.71 (m, 2H), 2.46 (s, 3H), 2.22-1.96 (m, 2H), 2.01-1.93 (m, 4H), 1.80-1.74 (m, 1H), 1.69-1.65 (m, 1H), 1.59-1.52 (m, 2H), 1.42 (s, 3H), 1.35-1.33 (m, 2H), 1.32 (s, 3H), 1.17 (m, 1H), 1.08 (s, 3H). ^{13}C -NMR (400 MHz, CDCl_3) δ 192.50, 167.27, 145.11, 133.07, 130.14, 129.75, 117.39, 81.88, 61.66, 41.67, 37.09, 35.57, 32.83, 31.41, 30.94, 27.68, 24.87, 23.15, 21.81, 20.71. *Data is for a mixture of diastereomers. Due to peak overlap, multiplicity and integration cannot be accurately determined for individual isomers. HRMS (m/z): $[\text{M}]^+$ calcd for $\text{C}_{23}\text{H}_{30}\text{O}_4\text{S}$, 402.1865; found 402.1871.

Compound 19

In a 3-neck, round-bottom flask equipped with a stir bar and water-cooled condenser, citral (3.670 g, 23.6 mmol) was dissolved in 200 mL of toluene. Orcinol (2.500 g, 20.1 mmol) was added followed by EDDA (0.725 g, 4.02 mmol). The reaction was refluxed for 6 hours, after which the solvent was removed *in vacuo*. The oily residue was purified by column chromatography over silica gel eluting with hexane/ethyl acetate (10:1) yielding **19** (3.043 g, 59% yield). ¹H-NMR (300 MHz, CDCl₃) δ 6.64 (d, 1H), 6.26 (s, 1H), 6.13 (s, 1H), 5.50 (d, 1H), 5.25 (bs, 1H), 5.11 (t, 1H), 2.21 (s, 3H), 2.13-2.10 (m, 2H), 1.72-1.65 (m, 2H) 1.68 (s, 3H), 1.60 (s, 3H), 1.39 (s, 3H). ¹³C-NMR (400 MHz, CDCl₃) δ 159.35, 155.07, 137.31, 114.72, 110.84, 103.55, 102.63, 63.72, 55.35, 49.51, 35.85, 33.15, 28.37, 27.94, 22.89, 19.06, 15.15. HRMS (m/z): [M+]⁺ calcd for C₁₇H₂₂O₂, 258.1620; found 258.1603.

Compound 20

In a 3-neck, round-bottom flask equipped with a stir bar and water-cooled condenser, citral (368 mg, 2.42 mmol) was dissolved in 12 mL of toluene. Orcinol (300 mg, 2.42 mmol) was added followed by p-toluenesulfonic acid (42 mg, 0.2417 mmol). The reaction was refluxed overnight. The reaction was washed once with saturated KHCO₃, followed by washing twice with DI H₂O. After the organic layer was dried over MgSO₄ and filtered, the solvent was removed *in vacuo*. The crude product was purified by column chromatography over silica gel eluting with hexane/ethyl acetate (5:1) yielding

20 (94 mg, 15% yield). ¹H-NMR (300 MHz, CDCl₃) δ 6.28 (s, 1H), 6.11 (s, 1H), 5.44 and 5.25 (bd, 1H), 4.76 (s, 1H), 3.18 (dd, 1H), 2.71 (td, 1H), 2.21, (s, 4H), 2.16-2.13 (m, 1H), 1.82-1.75 (m, 3H), 1.71 (s, 3H) 1.62 (s, 1H), 1.38 (s, 3H), 1.11 (s, 3H). ¹³C-NMR (400 MHz, CDCl₃) δ 155.13, 155.03, 138.01, 134.93, 119.53, 111.08, 110.57, 108.51, 77.42, 45.08, 36.24, 31.72, 28.04, 27.74, 23.68, 21.16, 18.66. *Data is for a mixture of cis/trans isomers. Due to peak overlap, multiplicity and integration cannot be accurately determined for individual isomers. Some experimental integration is higher due to impurities. HRMS (m/z): [M+]⁺ calcd for C₁₇H₂₂O₂, 258.1620; found 258.1611.

Compound 19

In a 3-neck, round-bottom flask equipped with a stir bar and water-cooled condenser, citral (1.500 g, 9.85 mmol) and 2,4-pentanedione (0.986 g, 9.85 mmol) was dissolved in 10 mL of THF. EDDA (0.443 g, 2.46 mmol) was then added, and the reaction was heated at 60°C for 1 hour. Hexane was added and the crude mixture washed once with mild aqueous acid and twice with DI H₂O. After the organic layer was dried over MgSO₄ and filtered, the solvent was removed *in vacuo*. The crude product was dissolved in EtOAc and passed over a small silica plug. Dry silica was added to the resulting solution was mounted onto silica, and the solvent removed *in vacuo*. The solid was placed in a large drying tube equipped with a stir bar and the reaction was heated under vacuum at 100°C for 1 hour. The crude product was removed from the silica by washing with EtOAc. This solvent was removed *in vacuo*. The residue was recrystallized in hexane to yield **19** (3.833 g, 83%). ¹H-NMR (300 MHz, CDCl₃) δ 5.34 and 5.45 (m, 1H), 3.31 (bs,

1H), 2.29 (s, 3H), 2.03 (d, 1H), 1.98 and 1.99 (s, 3H), 1.95-1.93 (m, 2H), 1.81-1.79 (cm, 3H), 1.64 (s, 3H), 1.60 (d, 1H), 1.32 (s, 3H), 1.27 (s, 3H). ¹³C-NMR (400 MHz, CDCl₃) δ 201.58, 155.40, 135.89, 121.18, 114.69, 39.90, 32.34, 30.78, 29.86, 25.71, 25.59, 23.76, 20.25, 20.22. *Data is for a mixture of cis/trans isomers. Due to peak overlap, multiplicity and integration cannot be accurately determined for individual isomers. Some experimental integration is higher due to impurities. HRMS (m/z): [M+]⁺ calcd for C₁₅H₂₂O₂, 234.1620; found 234.1615.

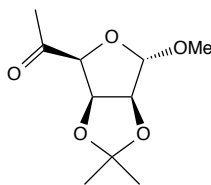
Compound 21

19 (150 mg, 0.640 mmol) was dissolved in 2 mL of an ethanolic sodium hydroxide solution in a vial. Benzaldehyde (68 mg, 0.640 mmol) was added, and the reaction was stirred at room temperature for 1 hour. Diethyl ether was added and the reaction mixture was washed twice with dilute acid solution and twice with DI H₂O. The organic layer was passed through a small silica plug, and after the solvent was removed *in vacuo* yielding **21** (152 mg, 74% yield). ¹H-NMR (300 MHz, CDCl₃) δ 7.58–7.53 (m, 3H), 7.39-7.37 (m, 3H), 6.99-6.94 (d, 1H), 5.43-5.41 (m, 1H), 3.45 (bs, 1H), 1.98 and 1.97 (s, 5H), 1.90-1.82 (cm, 2H), 1.63 (m, 1H), 1.58 (s, 3H), 1.44 (s, 3H), 1.42 (s, 3H). ¹³C-NMR (400 MHz, CDCl₃) δ 194.73, 154.33, 142.12, 135.65, 135.37, 130.23, 129.07, 128.41, 127.62, 121.24, 113.65, 39.83, 32.38, 30.21, 26.03, 25.79, 23.67, 20.16, 20.06. *Data is for a mixture of cis/trans isomers. Due to peak overlap, multiplicity and integration cannot be accurately determined for individual isomers. HRMS (m/z): [M+]⁺ calcd for C₂₂H₂₆O₂, 322.1933; found 322.1921.

Appendix B

Atomic Coordinates of Compounds Found in Chapter 4

(Note: One example is presented in this appendix. The remainder can be found in the following reference: Wilmot, N. Ph.D. Thesis, University of California, Riverside, 2006.



Aldehyde Coordinates:

Spartan '04 Semi-Empirical Program: (PC/x86)

Release 121

MOLECULE044

28 70 42 126 0 1 70 0 RHF PM3

NOOPT C1

GEOMETRY

8	-0.5381677	2.0582860	2.6958658
6	0.3440161	3.4983851	0.5791544
6	1.7147865	1.6701522	-1.2516380
6	2.1252376	-0.7707150	0.2884710
6	0.7351247	-0.2916796	2.8360365
1	1.7162149	4.9043454	1.3406736
1	3.4395130	2.5361243	-2.0687116
1	4.1173062	-1.3756155	0.5334186
1	-0.7231123	-1.7287152	3.3238214
8	0.2570192	0.9193668	-3.3767227
8	0.9725646	-2.7231569	-1.1379391
6	-0.5569741	-1.6572638	-3.1119306
6	-0.0147199	-3.0679418	-5.5803792
1	-0.5636321	-5.0610793	-5.4184819
1	1.9947826	-3.0059700	-6.08904547
1	-1.0886791	-2.2360519	-7.1476163
6	-3.3722274	-1.7913973	-2.4323276
1	-3.9880446	-3.7634744	-2.2513279
1	-4.5247606	-0.8970539	-3.9062494
1	-3.7903857	-0.8339044	-0.6376645
8	2.5807541	0.0760150	4.7249586
6	1.7671610	-0.4074358	7.2071975
1	3.4498203	0.0016598	8.3317015
1	1.2043188	-2.3850626	7.4619259
1	0.2116704	0.8333697	7.7783706
6	-1.9412646	4.8157809	-0.5976369
1	-3.7664455	3.8144786	-0.5180927
8	-1.7618772	6.8685537	-1.5754222